

Further Development of iCIPT2 for Strongly Correlated Electrons

Ning Zhang,[†] Wenjian Liu,^{*,‡} and Mark R. Hoffmann[¶]

[†]*Beijing National Laboratory for Molecular Sciences, Institute of Theoretical and Computational Chemistry, College of Chemistry and Molecular Engineering, Peking University, Beijing 100871, China*

[‡]*Qingdao Institute for Theoretical and Computational Sciences, Shandong University, Qingdao, Shandong 266237, China*

[¶]*Chemistry Department, University of North Dakota, Grand Forks, ND 58202-9024, U.S.A.*

E-mail: liuwj@sdu.edu.cn

Abstract

The efficiency of the recently proposed iCIPT2 [iterative configuration interaction (iCI) with selection and second-order perturbation theory (PT2); *J. Chem. Theory Comput.* 16, 2296 (2020)] for strongly correlated electrons is further enhanced (by up to 20×) by using (1) a new ranking criterion for configuration selection, (2) a new particle-hole algorithm for Hamiltonian construction over randomly selected configuration state functions (CSF), and (3) a new data structure for the quick sorting of the joint variational and first-order interaction spaces. Meanwhile, the memory requirement is also reduced greatly. As a result, this improved implementation of iCIPT2 can handle one order of magnitude more CSFs than the previous version, as revealed by taking the chromium dimer and an iron-sulfur cluster, $[\text{Fe}_2\text{S}_2(\text{SCH}_3)_4]^{2-}$, as examples.

1 Introduction

As pointed out recently,^{1,2} among the three components of electronic structure theory (i.e., relativity, correlation, and QED), it is correlation that is most challenging, especially for strongly correlated systems. Roughly speaking, a strongly correlated system features multiple open-shell orbitals or nearly degenerate electronic states thanks to the existence of a dense set of energetically adjacent frontier orbitals, such that there does not exist a single, leading component in the wave functions. Because of this, single-reference methods are bound to fail, especially for those low-spin states. Instead, multi-reference methods³⁻⁸ are needed even for a qualitative description of such states. A unanimous assumption underlying standard multi-reference methods is that the full many-electron Hilbert space can be decomposed into a model space P and the remaining complement $Q = 1 - P$, which are responsible for the static and dynamic components of the overall correlation, respectively. Then, according to when the static and dynamic correlations are handled, such methods can be classified into three families, viz. “static-then-dynamic”, “dynamic-then-static”, and “static-dynamic-static” (SDS).⁹ Given their great success in investigating low-lying electronic states of many chemical systems, it must be realized that such multi-reference methods still have strong limitations. For instances, it is by no means trivial to maintain the same model space, so as to produce smooth potential energy surfaces. Even if this can be achieved, there is no guarantee that the chosen model space is equally good for all geometries and all target states. Even more seriously, those states that have little projections in the chosen model space cannot well be described. Taking all these facts into account, one can classify chemical systems into weakly correlated (which can well be described by single-reference methods), moderately correlated (which can well be described by standard multi-reference methods with a moderate model space, typically much smaller than the complete active space (CAS) of 18 electrons in 18 orbitals), and strongly correlated (which require a large model space and are therefore beyond the capability of standard multi-reference methods). As a matter of

fact, the concept of model space loses its original meaning for the so-defined strongly correlated systems because the states in a large model space P and those formally in the orthogonal complement Q are heavily intersected in both energy and composition. In other words, the static and dynamic correlations are in such cases strongly entangled and interchangeable. Moreover, solving the large-model-space problem itself is already a heavy task, needless to say the subsequent treatment of dynamic correlation (NB: the larger the model space, the larger the first-order interacting space (FOIS)). So the question is how to design an adaptive method that can adapt to the variable static correlation automatically and can meanwhile handle the residual dynamic correlation efficiently. It appears that the most promising way to this end is to introduce some selection procedure, so as to build up progressively a compact yet accurate variational space P , in full accordance with the nature of the system under concern. In this spirit, a number of near-exact approaches have been designed in the past, including density matrix renormalization group (DMRG),¹⁰⁻²⁰ full configuration interaction (FCI) quantum Monte Carlo (FCIQMC),²¹⁻³⁰ cluster-analysis-driven FCIQMC,³¹ adaptive coupled-cluster (CC),³² full CC reduction,^{33,34} deterministically projected FCI,³⁵ many-body expanded FCI,³⁶⁻³⁹ incremental FCI,^{40,41} rank-reduction FCI,⁴² fast randomized interaction-based FCI,⁴³ intrinsic scaling-based correlation expansion,^{44,45} as well as selected CI (sCI).^{9,46-70} Among these, the sCI type of approaches, which are largely a revival of the very old ideas⁷¹⁻⁷⁵ in one way or another, are the simplest in structure and rival those more sophisticated approaches as shown in a recent blind test.⁷⁶ As the newest member of the sCI family, the iCIPT2 approach⁶⁶ proposed by the present authors, i.e., the combination of iterative CI (iCI)⁹ with selection and second-order perturbation theory (PT2) has a number of salient features:

- (1) Born from the restricted SDS framework⁶⁴ for strongly correlated electrons, iCI⁹ is a parameter-free, exact solver of the FCI eigenvalue problem. It constructs and diagonalizes a very small Hamiltonian matrix $\bar{\mathbf{H}}$ (see Sec. 2) at each macro/micro-iteration

but can converge quickly to the exact solutions. The major bottleneck of iCI lies therefore only in the construction of the Hamiltonian matrix \mathbf{H} in the basis of Slater determinants (SD) or configuration state functions (CSF) before contracted to $\bar{\mathbf{H}}$ for diagonalization. Since \mathbf{H} is extremely sparse, the combination of iCI with selection is a natural choice, leading to “selected iCI” (SiCI) as a near-exact solver of FCI. To be more practical, the (one-step) SiCI can be performed in two steps, with the first step accounting for the static correlation whereas the second step for a second-order perturbative treatment of the dynamic correlation. This can be achieved by a single parameter C_{min} , which controls the size of the variational space and hence the final accuracy. This scheme has been dubbed as iCIPT2.⁶⁶

- (2) The selection is carried out over the entire Hilbert space or a very large active space (which can in this context be viewed as a coarse-grained selection step). Those unimportant doubly excited orbital configurations (CFG) are first screened out based on the upper bounds of the elements of \mathbf{H} . After this integral-driven screening, the individual CSFs of a selected CFG are further selected using their approximate first-order coefficients. In short, although the selection is performed on individual CSFs, it is CFGs that are used as the organizing units. Given a coefficient pruning-threshold C_{min} , the selection of important CFGs/CSFs is performed iteratively until convergence.
- (3) At each iteration for the growth of wave function, the FOIS is decomposed into disjoint subspaces, so as to reduce memory requirement on one hand and facilitate parallelization on the other.
- (4) A new technique called TUGA (tabulated unitary group approach) is introduced to compute and reuse the basic coupling coefficients (BCC), i.e., the matrix elements of $U(n)$ generators over CSF pairs.
- (5) Because of the use of CSFs as the many-electron basis, full spin symmetry is always maintained, which is of vital importance for describing low-spin states of general

open-shell systems as well as subsequent perturbative treatment of spin-orbit couplings.

- (6) Upon termination of the selection, dynamic correlation is estimated by using the state-specific Epstein-Nesbet type of second-order perturbation theory (ENPT2).
- (7) The linear relationship between the total versus second-order correlation energies allows for an accurate extrapolation.

The present contribution amounts to further enhancing the efficiency of iCIPT2 by using (a) a new ranking criterion for the selection of CFGs/CSFs (see Sec. 4), (b) a new particle-hole algorithm for the construction and update of \mathbf{H} in the variational space (see Sec. 5), and (c) the Timsort algorithm^{77,78} for sorting the joint variational and first-order interacting spaces (see Sec. 6). Before these, we ought to outline the SDS family of methods in Sec. 2 and the essentials of TUGA in Sec. 3. A close comparison of TUGA with Table-CI⁷⁹⁻⁸² is also given in the latter, since they are both configuration-driven algorithms. The chromium dimer and an iron-sulfur cluster, $[\text{Fe}_2\text{S}_2(\text{SCH}_3)]_4^{2-}$, are finally taken as examples to reveal the efficacy of the improved implementation of iCIPT2 (see Sec. 7). The presentation is closed with concluding remarks in Sec. 8.

2 The SDS family of methods: SDSCI, SDSPT2, iCI, iCIPT2

The *restricted* “static-dynamic-static” (SDS) framework⁶⁴ for strongly correlated electrons gives rise first to the SDSCI approach, which is a minimal MRCI with the following form

for the wave function $|\Psi_i\rangle$ of state $i \in [1, N_P]$,

$$|\Psi_i\rangle = \sum_{k=1}^{mN_P} |\tilde{\Phi}_k\rangle C_{k,i}, \quad m = 3 \text{ or } 4, \quad (1)$$

$$|\tilde{\Phi}_k\rangle = |\Psi_k^{(0)}\rangle = \sum_{|J\nu\rangle \in P} |J\nu\rangle \bar{C}_{\nu,k}^{J(0)}, \quad k \in [1, N_P], \quad (2)$$

$$|\tilde{\Phi}_{k+N_P}\rangle = |\Psi_k^{(1)}\rangle = Q \frac{1}{E_k^{(0)} - H_0} QH |\Psi_k^{(0)}\rangle = \sum_{|J\nu\rangle \in Q} |J\nu\rangle \bar{C}_{\nu,k}^{J(1)}, \quad k \in [1, N_P], \quad (3)$$

$$|\tilde{\Phi}_{k+2N_P}\rangle = P_s |\Theta_k\rangle, \quad k \in [1, N_P], \quad (4)$$

$$|\tilde{\Phi}_{k+3N_P}\rangle = P_s |\Theta'_k\rangle, \quad k \in [1, N_P] \quad (\text{if } m > 3), \quad (5)$$

$$P = \sum_{J\nu}^{d_R} |J\nu\rangle \langle J\nu| = P_m + P_s, \quad P_m = \sum_{k=1}^{N_P} |\Psi_k^{(0)}\rangle \langle \Psi_k^{(0)}|, \quad Q = 1 - P. \quad (6)$$

Here, the first two sets of N_P functions $\{|\tilde{\Phi}_k\rangle\}$ are nothing but the zeroth-order (primary) and first-order (external) functions, respectively. To account for changes in the static correlation (described by $\{|\Psi_k^{(0)}\rangle\}_{k=1}^{N_P}$) due to the presence of dynamic correlation (described by $\{|\Psi_k^{(1)}\rangle\}_{k=1}^{N_P}$), N_P secondary (buffer) functions $\{|\Theta_k\rangle\}_{k=1}^{N_P}$, Eq. (4), are further introduced, which can be defined in a number ways. For instance, the *not-energy-biased* Lanczos-type functions (denoted as Buf(1)), $\{H|\Psi_k^{(1)}\rangle\}_{k=1}^{N_P}$, turn out to be very effective.⁶⁴ An alternative choice might be the second set of N_P zeroth-order functions $\{|\Psi_k^{(0)}\rangle\}_{k=N_P+1}^{2N_P}$ (denoted as Buf(0)) in the spirit of intermediate Hamiltonian theory, the first set of N_P second-order functions $\{|\Psi_k^{(2)}\rangle\}_{k=1}^{N_P}$ (denoted as Buf(2)) in the spirit of perturbation theory or the N_P approximate eigenvectors of the preceding iteration (denoted as Buf(3)) in the spirit of conjugate gradient theory.⁸³ While Buf(2) is very expensive, both Buf(0) and Buf(3) are very easy to handle because the Hamiltonian matrix elements can readily be evaluated.⁸³ As a matter of fact, Buf(0) and Buf(3) can be applied simultaneously without increasing the computational overhead. In this case, we will have $m = 4$ in Eq. (1). Otherwise, we have $m = 3$ in Eq. (1) with Buf(1) alone. The yet unknown expansion coefficients are to

be determined by the generalized secular equation

$$\bar{\mathbf{H}}\mathbf{C} = \mathbf{S}\mathbf{C}\mathbf{E}. \quad (7)$$

Since all the functions $\{|\tilde{\Phi}_k\rangle\}_{k=N_p+1}^{mN_p}$ are fully contracted (i.e., linear combinations of the CSFs $\{|\nu\rangle\}$ generated from CFGs $\{|J\rangle\}$) and are specific to the primary state $|\Psi_k^{(0)}\rangle$, the dimension of Eq. (7) is just 3 (or 4) times the number (N_p) of target states, no matter how many electrons and how many orbitals are correlated. Although restricted as such, it has been shown⁸⁴ that SDSCI is a very effective variational method for both ground and excited states. Two extensions of SDSCI have been considered so far, SDSPT2^{64,65} and iCI,⁹ both with Buf(1) alone. The former amounts to replacing the QHQ block of the Hamiltonian matrix in Eq. (7) with QH_0Q . Different from most variants of multi-reference second-order perturbation theory (MRPT2), the CI-like SDSPT2 treats single and multiple states in the same way and is particularly advantageous when a number of states are nearly degenerate, thanks to the efficacy of the secondary states in revising the coefficients of the primary states. In contrast, iCI takes the solutions of Eq. (7) as new primary states $\{|\Psi_k^{(0)}\rangle\}_{k=1}^{N_p}$ and repeats the SDS procedure (1) until convergence. Clearly, each iteration (defined as macro-iteration) accesses a space that is higher by two ranks than that of the preceding iteration. Up to $2i$ -tuple excitations (relative to the initial primary space) can be accessed if i macro-iterations are carried out. A few micro-iterations j can be invoked at each macro-iteration so as to relax the contraction coefficients. As such, every iCI(i, j) corresponds to a physically meaningful model. It has been shown both theoretically and numerically that iCI can converge quickly from above to FCI even when starting with a very poor initial guess. More generally, iCI can be viewed as a particular sequential, exact partial diagonalization of a huge matrix, by getting first the roots of one portion of the matrix and then those of an enlarged portion, until the full matrix, whereas its micro-iterations can be generalized to an iterative vector interaction (iVI) approach⁸³ for

the roots of a given matrix treated as a whole. Again, each iteration of iVI constructs and diagonalizes a $mN_p \times mN_p$ matrix ($m = 3$ or 4) in the form of Eq. (7). In particular, by combining with the energy-vector following technique, iVI can directly access interior roots belonging to a predefined window, without knowing the number and characters of the roots.⁸⁵

As stated before, iCIPT2 amounts to splitting iCI into two steps, the first of which accounts for the static correlation by selecting important CFGs/CSFs in an iterative manner, whereas the second of which accounts for the residual dynamic correlation via a second-order perturbation theory. It is the improvement of iCIPT2 that is under concern here.

3 TUGA

The very first issue pertinent to iCIPT2 is how to evaluate the Hamiltonian matrix elements over randomly selected CSFs $\{|J\nu\rangle\}$. In this context, the configuration-driven Table-CI approach⁷⁹⁻⁸² may be a possible choice. However, it involves line-up permutations of open-shell orbitals, which become ineffective for CFGs of many open-shell orbitals (say, > 10). To avoid such line-up permutations, we have introduced a “tabulated unitary group approach” (TUGA)⁶⁶ (originally called “tabulated orbital configuration-based unitary group approach”). Since the UGA⁸⁶⁻⁸⁸ is itself rather involved, we here recapitulate the essentials of TUGA. The first step is to break the spin-free, second-quantized Hamiltonian

$$H = \sum_{ij} h_{ij} E_{ij} + \frac{1}{2} \sum_{i,j,k,l} (ij|kl) e_{ij,kl}, \quad (8)$$

$$E_{ij} = \sum_{\sigma} a_{i\sigma}^{\dagger} a_{j\sigma} = E_{ji}^{\dagger}, \quad (9)$$

$$\begin{aligned} e_{ij,kl} &= \sum_{\sigma,\tau} a_{i\sigma}^{\dagger} a_{k\tau}^{\dagger} a_{l\tau} a_{j\sigma} = E_{ij} E_{kl} - \delta_{jk} E_{il} = \{E_{ij} E_{kl}\} \\ &= \{E_{kl} E_{ij}\} = e_{kl,ij} = e_{ji,lk}^{\dagger} \end{aligned} \quad (10)$$

into a form that is consistent with the diagrams employed in the UGA⁸⁷ for the BCC between CSFs. Specifically,

$$H = H_1^0 + H_2^0 + H_1^1 + H_2^1 + H_2^2, \quad (11)$$

$$H_1^0 = \sum_i h_{ii} E_{ii}, \quad (12)$$

$$H_1^1 = \sum_{i<j} h_{ij} E_{ij} + \sum_{i>j} h_{ij} E_{ij}, \quad (13)$$

$$H_2^0 = \frac{1}{2} \sum_i (ii|ii) E_{ii} (E_{ii} - 1) + \sum_{i<j} [(ii|jj) E_{ii} E_{jj} + (ij|ji) e_{ij,ji}], \quad (14)$$

$$H_2^1 = \sum_{i \neq j} [(ii|ij) (E_{ii} - 1) E_{ij} + (ij|jj) E_{ij} (E_{jj} - 1)] \\ + \sum_{i \neq j \neq k} [(ij|kk) E_{ij} E_{kk} + (ik|kj) e_{ik,kj}], \quad (15)$$

$$H_2^2 = \sum_{i \leq k} \sum'_{j \leq l} [2^{-\delta_{ik}\delta_{jl}} (ij|kl) e_{ij,kl} + (1 - \delta_{ik})(1 - \delta_{jl})(il|kj) e_{il,kj}], \quad (16)$$

where the superscripts 0, 1, and 2 in H_i ($i = 1, 2$) indicate that the terms contribute to the Hamiltonian matrix elements over two CFGs that are related by zero, single, and double excitations, respectively, whereas the prime in Eq. (16) indicates that $\{j, l\} \cap \{i, k\} = \emptyset$. For two identical CFGs $|I\rangle$, the Hamiltonian matrix elements can be calculated most efficiently as⁶⁶

$$\langle I\mu | H_1^0 + H_2^0 | Iv \rangle = \delta_{\mu\nu} \left\{ \frac{1}{2} \sum_i n_i^R [h_{ii} + \epsilon_i + (n_i^R - 2)g_{ii}] + \sum_i \Delta_i^I [\epsilon_i + (n_i^R - 1)g_{ii}] \right. \\ \left. + \sum_{i \leq j} \Delta_i^I g_{ij} \Delta_j^I \right\} + \sum_{i < j} (ij|ji) \langle I\mu | e_{ij,ji}^1 | Iv \rangle \delta(n_i^I, 1) \delta(n_j^I, 1), \quad (17)$$

$$f_{ij} = h_{ij} + \sum_k n_k^R [(ij|kk) - \frac{1}{2}(ik|kj)], \quad (18)$$

$$\epsilon_i = f_{ii} = h_{ii} + \sum_k n_k^R g_{ik}, \quad g_{ik} = (ii|kk) - \frac{1}{2}(ik|ki) = g_{ki}, \quad (19)$$

$$\Delta_i^I = n_i^I - n_i^R, \quad (20)$$

where $\{n_i^R\}$ are the occupation numbers of the spatial orbitals of a common reference CFG $|R\rangle$ (either Hartree-Fock (HF) or restricted open-shell HF). The superscript 0 or 1 in $e_{ij,kl}$ (see Eq. (17)) refers to the intermediate angular momentum X due to the coupling of two spin- $\frac{1}{2}$ functions. If $|I\rangle = E_{ij}|J\rangle$, the corresponding Hamiltonian matrix elements read (under the Yamanouchi-Kotani (YK) phase⁸⁷)

$$\begin{aligned}
\langle I\mu|H_1^1 + H_2^1|J\nu\rangle &= \langle I\mu|E_{ij}|J\nu\rangle \left[f_{ij} + \sum_k \Delta_k^J [(ij|kk) - \frac{1}{2}(ik|kj)] \right. \\
&\quad \left. + \frac{1}{2}n_i^J(ii|ij) + (\frac{1}{2}n_j^J - 1)(ij|jj) \right] \\
&\quad + \sum_{k \in \text{exterior open}} (ik|kj) \langle I\mu|e_{ik,kj}^1|J\nu\rangle \\
&\quad + \sum_{k \in \text{interior open}} (ik|kj) \left[\frac{1}{2} \langle I\mu|E_{ij}|J\nu\rangle + \langle I\mu|E_{kj}E_{ik}|J\nu\rangle \right], \tag{21}
\end{aligned}$$

where ‘exterior open’ and ‘interior open’ emphasize that level k belongs to the non-overlapping ($k < \min(i, j)$ or $k > \max(i, j)$) and overlapping ($\min(i, j) < k < \max(i, j)$) cases, respectively, and is singly occupied. On the other hand, if $|I\rangle = e_{ij,kl}|J\rangle$ subject to $\{j, l\} \cap \{i, k\} = \emptyset$, the Hamiltonian matrix elements read

$$\langle I\mu|H_2^2|J\nu\rangle = \left[2^{-\delta_{ik}\delta_{jl}}(ij|kl) \langle I\mu|e_{ij,kl}|J\nu\rangle + (1 - \delta_{ik})(1 - \delta_{jl})(il|kj) \langle I\mu|e_{il,kj}|J\nu\rangle \right]. \tag{22}$$

At this stage two important points can be observed:

- (1) Thanks to the conjugacy (bra-ket inversion) relations $\langle I\mu|E_{ij}|J\nu\rangle = \langle I\mu|E_{ij}|J\nu\rangle^* = \langle J\nu|E_{ji}|I\mu\rangle$ and $\langle I\mu|e_{ij,kl}|J\nu\rangle = \langle I\mu|e_{ij,kl}|J\nu\rangle^* = \langle J\nu|e_{ji,lk}|I\mu\rangle$ in the absence of spin-orbit couplings, only generators E_{ij} with $i > j$ and $e_{ij,kl}$ with $k \geq i$ and $k > l \geq j$ need to be considered explicitly. They correspond to the s2, cx and dx ($x \in [1, 7]$) types of diagrams shown in Figs. 2 and 3 of Ref. 66. More specifically, the s2, c4, c6 and d2 diagrams are required for the evaluation of Eq. (21), while the other cx and dx types of diagrams are needed for the evaluation of Eq. (22). Once such BCCs are available,

those conjugate ones can be obtained simply by matrix transpose.

- (2) The BCCs $\langle I\mu|E_{ij}|J\nu\rangle$ and $\langle I\mu|e_{ij,kl}|J\nu\rangle$ depend only on the relative occupations of the CFG pair (I, J) but not on the individual orbitals $\{i, j, k, l\}$. Moreover, the common zero or doubly occupied orbitals need not be considered explicitly because their segment values are just one under the YK phase. Therefore, they can be rewritten as $\langle I\mu|E_{\bar{i}\bar{j}}|J\nu\rangle$ and $\langle I\mu|e_{\bar{i}\bar{j},\bar{k}\bar{l}}|J\nu\rangle$, respectively, in terms of the reduced orbital indices (ROI) $\{\bar{i}, \bar{j}, \bar{k}, \bar{l}\}$ after deleting the common zero or doubly occupied orbitals. Note that the ROIs have one-to-one correspondence with the original orbital indices (see the example in Table 1). This way, the same BCCs can be used for very many integrals sharing the same ROIs.

After deleting the common zero or doubly occupied orbitals in the bra and ket CFGs, we are left with seven occupation patterns, each of which can be assigned a code number as shown in Table 2. Every pair of CFGs can therefore be characterized by a reduced occupation table (ROT) consisting of two sequences, ROT_Orb and ROT_Code. The former records the orbital indices to fetch molecular integrals, whereas the latter records the corresponding code sequence (e.g., (012430) for the example shown in Table 1) to determine the generators, with the following rules: (1) if CFG $|I\rangle$ arises from $|J\rangle$ by exciting one electron from orbital j to orbital i , \bar{j} would then correspond to code 2 or 4, while \bar{i} to code 1 or 3 because of the relations $n_j^I = n_j^J - 1$ and $n_i^I = n_i^J + 1$. (2) If CFG $|I\rangle$ arises from $|J\rangle$ by exciting two electrons from orbitals j and l ($\geq j$) to orbitals i and k ($\geq i$) [NB: $\{i, k\} \cap \{j, l\} = \emptyset$], \bar{j} and \bar{l} ($\geq \bar{j}$) would correspond to code 2, 4 or 6, while \bar{i} and \bar{k} ($\geq \bar{i}$) to code 1, 3 or 5 because of the relations $n_j^I = n_j^J - 1$, $n_l^I = n_l^J - 1$, $n_i^I = n_i^J + 1$ and $n_k^I = n_k^J + 1$. Codes 6 and 5 further imply $\bar{j} = \bar{l}$ and $\bar{i} = \bar{k}$, respectively. (3) If $\bar{i} < \bar{j}$ in $E_{\bar{i}\bar{j}}$ or $\bar{k} < \bar{l}$ in $e_{\bar{i}\bar{j},\bar{k}\bar{l}}$, a bra-ket inversion should be invoked when calculating the BCCs in terms of the diagrams documented in Table 3. To search and sort the code sequences efficiently, each ROT_Code will be converted to an array of 64-bit integers (3 bits per code). It is clear that, to reuse the BCCs efficiently, the CFG pairs with the same ROT_Code

must be grouped together. Instead of the red-black tree type of bilinear search employed before,⁶⁶ we adopt here an array-based sorting algorithm: (a) generate all connected CFG pairs and store them in one array; (b) loop over each CFG pair and identify its ROT_Orb and ROT_Code; (c) sort the array based on ROT_Code. This way, those CFG pairs sharing the same ROT_Code (and hence the same BCCs) are adjacent to each other and form a segment in the array. To expedite the sorting process, the code sequences can further be characterized by their lengths and category numbers (CN) defined in Table 3. The latter just number different ranges of the generators (CN = 0 for singles and CN \in [1,7] for doubles) and are hence directly related to the diagrams required for the evaluation of the BCCs. This new sorting algorithm is significantly faster than the red-black trees employed before, although the latter is not really expensive for this purpose.

Table 1: Illustration on the reduced orbital indices (ROI)

OrbIndx	0	1	2	3	4	5	6	7
bra occ	1	0	1	0	2	1	2	1
ket occ	1	0	0	1	2	2	1	1
ROT_Orb	0	×	2	3	×	5	6	7
ROI	$\bar{0}$	×	$\bar{1}$	$\bar{2}$	×	$\bar{3}$	$\bar{4}$	$\bar{5}$
ROT_Code*	0	×	1	2	×	4	3	0

* See Table 2.

Table 2: Code numbers for the relative occupation patterns of CFG pairs

bra occ	1	1	0	2	1	2	0	0	2
ket occ	1	0	1	1	2	0	2	0	2
code	0	1	2	3	4	5	6	×	×

To be compatible with the desired generator ranges, we have to represent and store properly the CFGs and corresponding CSFs. A CFG can first be represented by an array of occupation numbers, $\text{Occ}[i]=n_i, i \in [0, N_{orb} - 1]$, with N_{orb} being the total number of spatial orbitals. The comparison of a CFG pair can then be performed efficiently with Algorithm 3 presented previously.⁶⁶ A CFG pair (I, J) is said to be singly or doubly connected if $|I\rangle$ can be obtained by exciting one or two electrons from $|J\rangle$. CFG $|I\rangle$ is stored

Table 3: Correspondence between UGA diagrams and category numbers (CN) of code sequences recorded in ROT_code

CN	Generator	Range	Diagram ^a	\tilde{H}^{IJ} ^b
0	E_{ij} $e_{ik,kj}^1$	$i > j$	s2	$\max((ij kl) + (il kl) , \sqrt{3} (ij kl) - (il kj))$
		$i > j > k$	c4	
		$k > i > j$	c6	
		$i > k > j$	d2	
1	$e_{ij,kl}$ $e_{il,kj}$	$k > l > j > i$	c1	
			c3	
2	$e_{ij,kl}$ $e_{il,kj}$	$k > l > i > j$	d1	
			c5	
3	$e_{ij,kl}$ $e_{il,kj}$	$k > i > l > j$	d3	
			d5	
4	$e_{ij,kj}$	$k > j > i$	c2	$2 (ij kj) $
5	$e_{ij,kj}$	$k > i > j$	d4	
6	$e_{il,ij}$	$i > l > j$	d6	$2 (il ij) $
7	$e_{ij,ij}$	$i > j$	d7	$ (ij ij) $

^a See Figs. 1-3 in Ref. 66.

^b Estimates of $|\langle I\mu|H_2^2|J\nu\rangle|$, which are upper bounds⁶⁶ for $\text{CN} \in [4, 7]$, exact for $\text{CN} \in [1, 3]$ if $|I\rangle$ or $|J\rangle$ is a closed shell CFG, but not guaranteed to be upper bounds for $\text{CN} \in [1, 3]$ if both $|I\rangle$ and $|J\rangle$ are open-shell CFGs (NB: slight deviations from the upper bounds can be taken care of by adjusting C_{min}).

preceding CFG $|J\rangle$ (i.e., $I < J$) if and only if $n_p^I > n_p^J$ for $p = \max\{x | n_x^I \neq n_x^J\}$. A more compact representation of CFGs is to use two bits to store the occupancy number of each spatial orbital. Specifically, $(00)_2$, $(01)_2$ and $(11)_2$ are used for $n_i = 0, 1$, and 2 , respectively. A CFG can then be represented by an array, `OrbOccBinary`, of 64-bit integers. This representation was used for both bra and ket CFGs in our previous implementation. Now it is discovered that the single occupancy in the bra CFG can be represented by $(10)_2$ instead of $(01)_2$, so as to make the identification of `ROT_Code` more efficiently. As can be seen from Table 4, the bitwise XOR operations on the so-defined binary occupation codes (BOC) always give $(00)_2$ for common zero or doubly occupied orbitals, such that the identification of `ROT_Code` can be achieved based fully on bit operations. Such double representation requires $M_{CFG} = 2 \times 8 \left(\lfloor \frac{N_{orb}-1}{32} \rfloor + 1 \right)$ bytes of memory for storing a CFG.

Table 4: Bitwise XOR operations on binary occupation codes (BOC)

Bra Occ	BOC	Ket Occ	BOC	XOR
0	$(00)_2$	0	$(00)_2$	$(00)_2$
2	$(11)_2$	2	$(11)_2$	$(00)_2$
1	$(10)_2$	1	$(01)_2$	$(11)_2$
0	$(00)_2$	1	$(01)_2$	$(01)_2$
0	$(00)_2$	2	$(11)_2$	$(11)_2$
1	$(10)_2$	0	$(00)_2$	$(10)_2$
1	$(10)_2$	2	$(11)_2$	$(01)_2$
2	$(11)_2$	0	$(00)_2$	$(11)_2$
2	$(11)_2$	1	$(01)_2$	$(10)_2$

A CFG $|I\rangle$ can generate $N_{S,S}^I$ genealogically coupled CSFs $\{|I\mu\rangle\}_{\mu=0}^{N_{S,S}^I-1}$ of total spin S , with $N_{S,S}^I$ being

$$N_{S,M=S}^I = \frac{2S+1}{\frac{1}{2}N_o^I + S + 1} C_{N_o^I}^{\frac{1}{2}N_o^I - S}, \quad (23)$$

where N_o^I is the (seniority) number of open-shell orbitals in CFG $|I\rangle$. Such CSFs are characterized uniquely by the Shavitt step number⁸⁹ sequences $\{(d_0^\mu d_1^\mu \dots)\}_{\mu=0}^{N_{S,S}^I-1}$, which can be arranged in a lexical order (i.e., $|I\mu\rangle$ precedes $|I\nu\rangle$ if and only if $d_p^\mu < d_p^\nu$ for

$p = \min\{x | d_x^\mu \neq d_x^\nu\}$, so as to fix the relative ordering μ uniquely. A 32-bit integer is required to store the relative ordering of CSFs $\{|I\mu\rangle\}$. Since both its BOC and lexical order have to be stored, the memory requirement for storing a CSF is $M_{CFG} + 8$ bytes due to memory alignment. The ordering of CSFs is defined as follows: if CSF $|I\mu\rangle$ and $|J\nu\rangle$ stem from the same CFG, then $|I\mu\rangle < |J\nu\rangle$ if $\mu < \nu$; otherwise, let Occ_Y ($Y = I, J$) be the corresponding occupation array of CFG $|Y\rangle$ and $i = \arg \max_j \{Occ_I[j] \neq Occ_J[j]\}$, then $|I\mu\rangle < |J\nu\rangle$ if $Occ_I[i] > Occ_J[i]$. In view of Eq. (23), a large number of CSFs can be generated from a CFG of high seniority N_o^I but only a few of them may contribute discernibly. Therefore, it is absolutely necessary to do individual selections of CSFs.

After the above detailed description of TUGA, a gross comparison with the Table-CI approach^{79–82} is in order. Although both are configuration-driven algorithms for calculating the Hamiltonian matrix elements over randomly selected CSFs, they actually differ significantly. First of all, Table-CI is closely related to the symmetric group approach (SGA)⁹⁰ in view of its explicit tabulation of line-up permutations, whereas TUGA is plainly an implementation of the UGA,^{86–88} in terms of the tabulated ROTs rather than the famous graphical representation^{89,91} (which is efficient only for well-structured wave functions). Secondly, TUGA and Table-CI differ in the handling of open-shell orbitals. While Table-CI always defines CFGs with doubly occupied orbitals sitting together and open-shell orbitals sitting together (which involves reordering of the orbitals for each CFG), TUGA adopts a universal orbital ordering defined in the very beginning. The common open-shell orbitals are eliminated in Table-CI by virtue of line-up permutations, leaving a relatively small number of unique interaction patterns between SDs resulting from non-identical open-shell orbitals. However, the BCCs between CSFs are dependent on the relative positions of common open-shell orbitals. Therefore, they are not permuted in TUGA but stay where they are after deleting the common zero or doubly occupied orbitals. This increases merely the lengths of code sequences but not the number of ROTs (NB: every CFG pair corresponds to a ROT). In essence, the ROTs in TUGA play the same

role in classifying unique interacting CFG pairs at the integral level as the Tables defined in Table-CI. The former are calculated on an as-needed basis, whereas the latter, characterized by a number of parameters (i.e., ΔK , P , Q , and R determined by the relative occupations of CFG pairs; see Ref. 82 for more details), are created and stored in advance. Thirdly, TUGA evaluates the Hamiltonian matrix elements directly between CSFs, whereas Table-CI has to assemble them via transformations of those between SDs (which can be viewed as an effective means to avoid the overly complicated matrix elements of line-up permutations Q over CSFs, as required by the genuine SGA⁹⁰).

In short, TUGA has been based on the single, simple fact that the segment values for common zero or doubly occupied orbitals are always one under the YK phase,⁸⁷ such that the BCCs are determined solely by those common open-shell orbitals or orbitals with different occupancy numbers (which are encoded in the code sequences) and can be calculated directly through products of their segment values.

4 Selection of CSFs

The aim of selection is to find a better variational space P by feeding in a guess space P_0 . This can be achieved in two steps, ranking and pruning. In the ranking step, proper rank values for the CSFs in the FOIS Q ($= 1 - P_0$) will be evaluated. Those CSFs with rank values larger than the given ranking-threshold are put into P_0 , leading to an expanded space P_1 . In the pruning step, the Hamiltonian matrix in P_1 is first constructed and diagonalized. Those CSFs with coefficients smaller in absolute value than the given pruning-threshold are then discarded, so as to reduce P_1 to P . The procedure is repeated until the energies obtained by diagonalizing P and P_0 are sufficiently close. Such a two-step selection scheme has been adopted by most sCIs. Yet, a number of refinements has been introduced in our own implementation:⁶⁶

(1) A combined integral- and coefficient-driven algorithm is used for the selection, viz.

prior to the selection of individual CSFs with their (approximate) first-order coefficients as rank values, a integral-driven screening of unimportant, doubly connected CFG pairs is first carried out based on upper bounds \tilde{H}^{IJ} of $\langle I\mu|H_2^2|J\nu\rangle$ (which are independent of CSFs, see Table 3).

- (2) To minimize the usage of memory, an increment access of the Q space is invoked, with a dynamically adjusted integral-threshold $\varepsilon_k (= \frac{1}{2}\varepsilon_{k-1})$. For a given ε_k of iteration k (i.e., $Q[\varepsilon_k]$), the selection is repeated until $P[\varepsilon_k]$ and $P_0[\varepsilon_k]$ are sufficiently similar in composition (i.e., $\frac{|P_0[\varepsilon_k] \cap P[\varepsilon_k]|}{|P_0[\varepsilon_k] \cup P[\varepsilon_k]|} \geq 0.95$).
- (3) Natural orbitals (NO) are also generated dynamically (i.e., for each converged $P[\varepsilon_k]$; for more details, see Algorithm 4 in Ref. 66).
- (4) A residue-based algorithm^{62,63,92} is used for establishing the connections between randomly selected CFGs and CSFs.
- (5) The diagonalization of Hamiltonian matrix is performed with the iVI-Buf(0+3) approach,^{83,85} which has the potential to access directly the roots of a given energy window.
- (6) The size of the resulting variational space $P[\varepsilon_k = 0]$ is controlled by a single parameter C_{min} (coefficient pruning-threshold), for other parameters have been fixed to conservative values.

It has been demonstrated that the above selection can generate a very compact yet accurate variational space. However, its efficiency is not yet satisfactory because of the following reasons related to the first four points above: (a) the adopted ranking criterion is too good (and hence expensive) for the purpose of selection. (b) Although the incremental access of the Q space is very effective in reducing memory requirement and does not affect the final result, it does result in additional iterations and hence slow down the selection procedure. (c) The generation of NOs and hence transformation of integrals are

performed too many times, which is unnecessary. (d) The residue-based algorithm is not optimal for identifying the connections between the CFGs in P . In particular, it does not allow for an easy construction of the Hamiltonian matrix in CSR format. To resolve these issues, we here introduce a simpler ranking criterion, remove the incremental access of Q , simplify the generation of NO, and replace the residue-based algorithm with a particle-hole algorithm for Hamiltonian construction (see Sec. 5).

In view of many-body perturbation theory (MBPT), the most rigorous ranking of a CSF $|I\mu\rangle \in Q$ is its first-order coefficient in absolute value

$$f(|I\mu\rangle, C_{min}) = \left| \frac{\sum_{|J\nu\rangle \in P_0} H_{\mu\nu}^{IJ} C_\nu^J}{E_0 - H_{\mu\mu}^{II}} \right| \geq C_{min}, \quad H_{\mu\nu}^{IJ} = \langle I\mu | H | J\nu \rangle, \quad (24)$$

which is to be called ‘CIPSI criterion’, with CIPSI standing for ‘configuration interaction with perturbative selection made iteratively’.⁷³ If those $|J\nu\rangle \in P_0$ with small coefficients are excluded from the sum in the numerator of Eq. (24), it may be termed ‘pruned CIPSI criterion’ or simply ‘ASCI criterion’, as adopted by adaptive sampling CI.⁶⁰ Noticing that the computational expense of Eq. (24) results from both the sum in the numerator and the evaluation of the denominator, a dramatically simplified criterion is considered in heat-bath CI (HBCI),⁵⁰ viz.,

$$f(|I\mu\rangle, |J\rangle, \epsilon_Q) = \max_\nu |H_{\mu\nu}^{IJ} C_\nu^J| \xrightarrow{\text{CSF} \rightarrow \text{SD}} \max_\nu |H_{\mu\nu} C_\nu| \geq \epsilon_Q, \quad (25)$$

in the basis of SDs though. This way, those determinants $\{|\mu\rangle\}$ that are doubly excited from $|v\rangle \in P_0$ are never accessed if $|H_{\mu\nu}| < \epsilon_Q/|C_\nu|$.⁹³ However, such integral-driven selection leads usually to a variational space that is much less compact than that by the coefficient-driven selection (24), particularly when a large basis set is used. A possible remedy to this is to introduce⁹⁴ an approximate denominator to condition (25), without sacrificing the efficiency. Our previous ‘iCI criterion’⁶⁶ amounts to combining *dynamically*

these integral- and coefficient-driven algorithms for selecting doubly excited CSFs, viz.,

$$f(|I\mu\rangle, \varepsilon_k, C_{min}) = \left| \frac{\sum_{J \in P_0^{(k)}} (\sum_{\nu, |J\nu\rangle \in P_0^{(k)}} H_{\mu\nu}^{IJ} C_{J\nu}^{J(k)})}{E^{(k)} - H_{\mu\mu}^{II}} \right| \geq C_{min}, \quad (26)$$

where ε_k is a dynamically adjusted integral-threshold and the summation over CFG $|J\rangle \in P_0^{(k)}$ is subject to the following condition

$$\max_{\nu} |\tilde{H}^{IJ} C_{J\nu}^{J(k)}| \geq \varepsilon_k = \frac{1}{2} \varepsilon_{k-1}, \quad |J\rangle \in P_0^{(k)}. \quad (27)$$

The original motivation for this particular criterion is to reduce memory usage as much as possible and meanwhile to end up with a variational space that is as compact as possible. It appears that both are not really necessary: the memory requirement in the PT2 step is much larger and a slight sacrifice of the compactness can be overcompensated by the dramatic gain in efficiency. Therefore, we introduce here a new ‘iCI criterion’, that is, for a given $|I\mu\rangle \in Q = 1 - P_0$, if there exists a $|J\rangle \in P_0$ for which $f(|I\mu\rangle, |J\rangle, C_{min})$ is true, then $|I\mu\rangle$ is selected. The boolean function $f(|I\mu\rangle, |J\rangle, C_{min})$ is defined as

(A) If $|I\rangle$ is identical with or singly excited from $|J\rangle$, then

$$f(|I\mu\rangle, |J\rangle, C_{min}) = \left(\max_{\nu} (|H_{\mu\nu}^{IJ} C_{J\nu}|) \geq C_{min} \right) \text{ and } \left(\max_{\nu} \left(\left| \frac{H_{\mu\nu}^{IJ} C_{J\nu}}{E_0 - H_{\mu\mu}^{II}} \right| \right) \geq C_{min} \right); \quad (28)$$

(B) If $|I\rangle$ is doubly excited from $|J\rangle$, then

$$f(|I\mu\rangle, |J\rangle, C_{min}) = \left(\max_{\nu} (|\tilde{H}^{IJ} C_{J\nu}|) \geq C_{min} \right) \text{ and } \left(\max_{\nu} (|H_{\mu\nu}^{IJ} C_{J\nu}|) \geq C_{min} \right) \\ \text{and } \left(\max_{\nu} \left(\left| \frac{H_{\mu\nu}^{IJ} C_{J\nu}}{E_0 - H_{\mu\mu}^{II}} \right| \right) \geq C_{min} \right). \quad (29)$$

Literally, for case (A), loop over all $|I\mu\rangle$ in Q and evaluate $H_{\mu\nu}^{IJ}$ for all CSFs $|J\nu\rangle \in P_0$. If

$\max_v (|H_{\mu\nu}^{IJ} C_{J\nu}|)$ is larger than C_{min} then evaluate $H_{\mu\mu}^{II}$; otherwise discard $|I\mu\rangle$. If $\max_v (|\frac{H_{\mu\nu}^{IJ} C_{J\nu}}{E_0 - H_{\mu\mu}^{II}}|)$ is larger than C_{min} then $|I\mu\rangle$ is selected. As for case (B), only those doubly excited CFGs $|I\rangle$ with \tilde{H}^{IJ} larger than $C_{min} / \max_v |C_{J\nu}|$ need to be generated (i.e., those unimportant ones are never touched, as illustrated in Fig. 1). For such $\{|I\rangle\}$, the remaining step is the same as case (A).

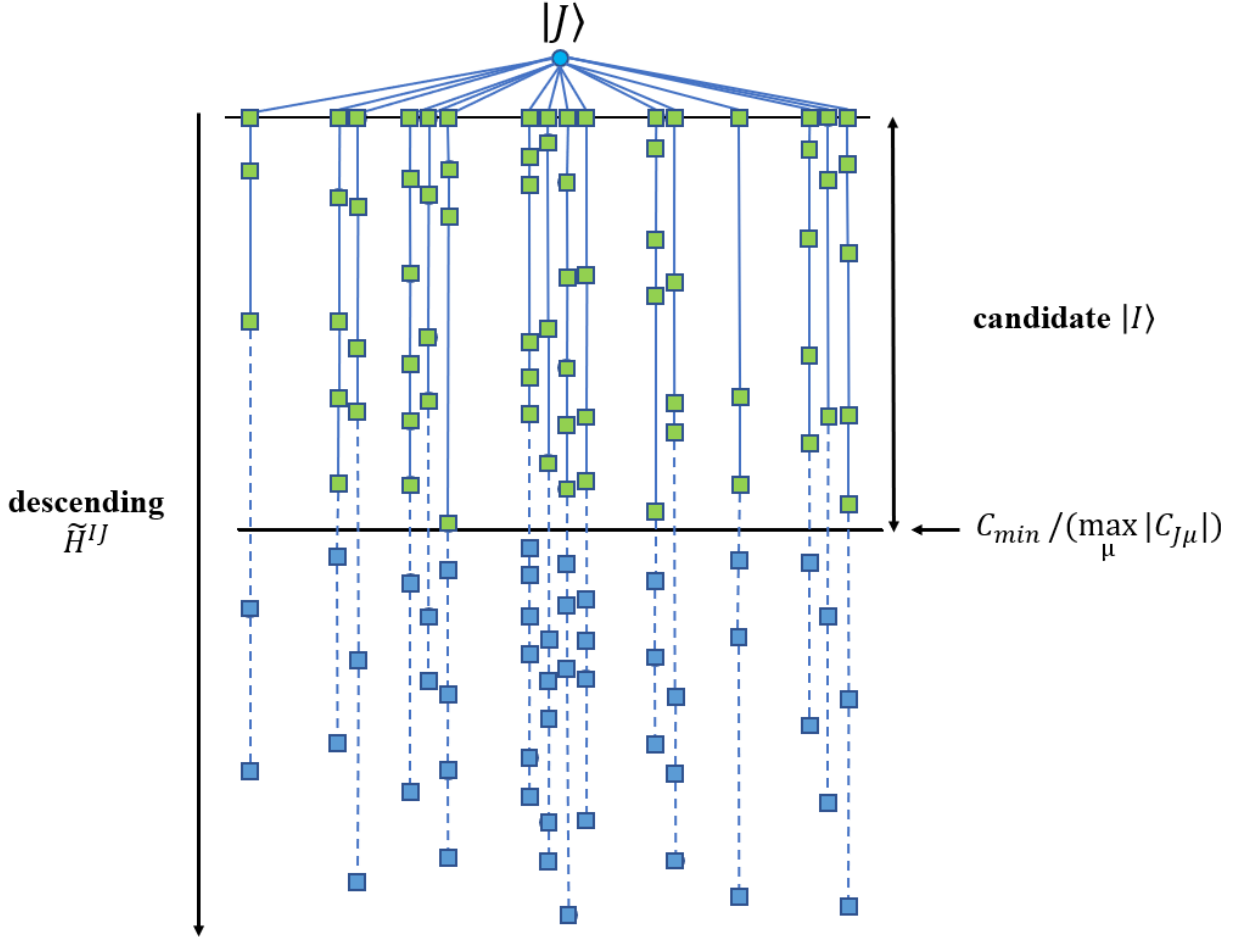


Figure 1: Screening of doubly excited configurations based on upper bounds.

It should be clear that, for the same C_{min} , the revised 'iCI criterion' (28)/(29) will yield a smaller number of CSFs than the original one (26)/(27), for the latter may accumulate those CSFs of small coefficients until the condition is fulfilled (cf. the second sum in Eq. (26)), whereas the former just picks up the CSF with the largest coefficient. Note in passing that, to be compared directly with this 'iCI criterion', the 'HBCI criterion' (25)

should be rewritten as

(a) If $|I\rangle$ is identical with or singly excited from $|J\rangle$, then

$$f(|I\mu\rangle, |J\rangle, C_{min}) = \max_{\nu} (|H_{\mu\nu}^{IJ} C_{J\nu}|) \geq C_{min}; \quad (30)$$

(b) If $|I\rangle$ is doubly excited from $|J\rangle$, then

$$f(|I\mu\rangle, |J\rangle, C_{min}) = \left(\max_{\nu} (|\tilde{H}^{IJ} C_{J\nu}|) \geq C_{min} \right) \text{ and } \left(\max_{\nu} (|H_{\mu\nu}^{IJ} C_{J\nu}|) \geq C_{min} \right), \quad (31)$$

which amounts to skipping the final step in Eqs. (28)/(29).

The overall selection procedure is illustrated in Fig. 2. Four additional points still deserve to be mentioned:

- (1) For multiple states, the selection will be carried out in a state-collective way. That is, the boolean function f_k defined in Eq. (24), (28)/(29) or (30)/(31) is examined for each state k and $|I\mu\rangle$ is selected if $\exists k$ and $|J\nu\rangle$ s.t. $f_k = \text{true}$.
- (2) Duplicates in the selected CSFs $\{|I\mu\rangle\} \in Q$ are removed as follows. The for-loop over CFGs $|J\rangle$ in P_0 is distributed among working threads. For each thread, once the memory usage has reached a given size (e.g., 2 GB), the selected CSFs $\{|I\mu\rangle\}$ are sorted immediately, with duplicates removed by a single loop. To expedite this, the CSFs are classified according to their seniorities and highest occupied orbitals. The surviving CSFs $\{|I\mu\rangle\}$ are then compared with those in P_0 to further remove the duplicates. Once the loop over $|J\rangle$ is done, the surviving CSFs $\{|I\mu\rangle\}$ from each thread are merged to the main thread and a final removal of duplicates is then executed.
- (3) The selection is terminated once the measure of composition similarity, $\frac{|P_0 \cap P|}{|P_0 \cup P|}$, exceeds the threshold S_P (e.g., 0.95).

(4) If desired, NOs can be generated in a partially dynamic manner, e.g., going from $C'_{min} = 4C_{min}$ to $2C_{min}$ and finally to C_{min} . For each C'_{min} , the above selection is performed to find the corresponding variation space P , from which the NOs can be generated. After integral transformation, the Hamiltonian matrix is reconstructed and diagonalized, with unimportant CSFs pruned. This extra step is important for the expansion coefficients of the wave function are affected by orbital rotations. The NOs generated this way usually give rise to a more compact variational space than those generated directly at the target C_{min} .

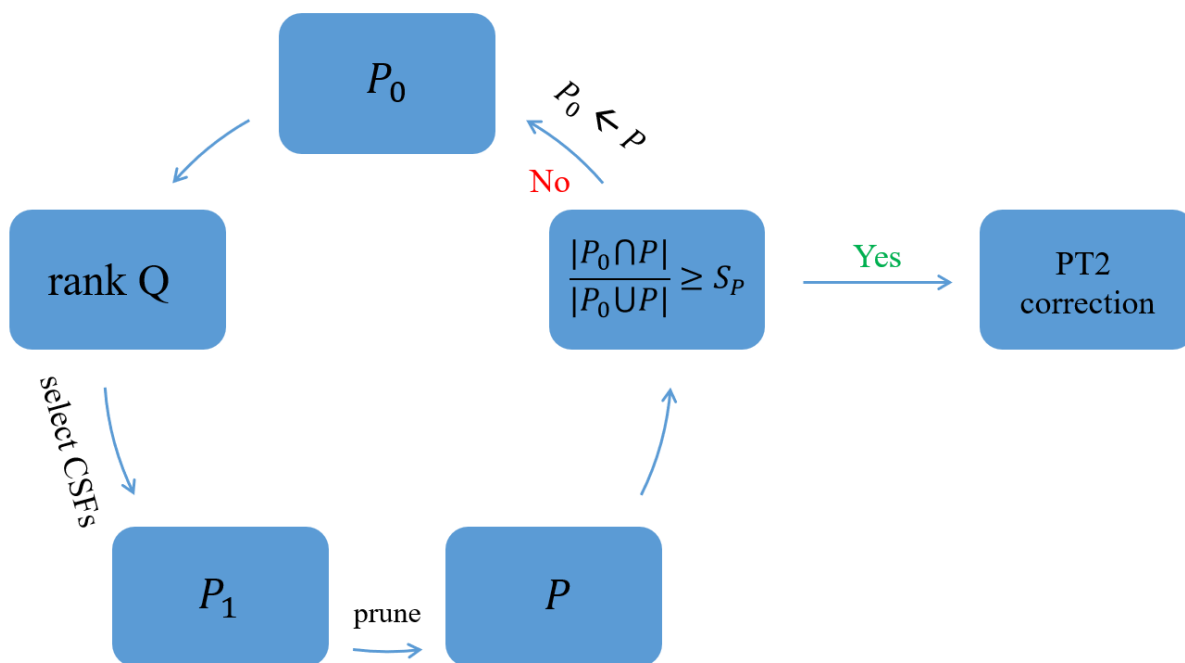


Figure 2: Flowchart for iCIPT2.

5 Connections between selected CSFs

Having identified the most important CSFs spanning space P , their connections must be established for constructing and updating the Hamiltonian matrix. In the previous implementation of iCIPT2,⁶⁶ we adopted the residue array-based algorithm.^{62,63,92} The

n th-order residues of an N_e -electron CFG $|I\rangle$ are those $(N_e - n)$ -electron CFGs that can be generated by removing n electrons from $|I\rangle$ in all possible ways. A nice point of residues lies in that they provide connection information on the parent CFGs. For instance, different CFG pairs sharing the same first-order residue (FOR) are identical or singly connected, while those sharing the same second-order residue (SOR) are identical, singly or doubly connected. However, for the purpose of constructing and updating the Hamiltonian matrix in the P space, the residues have some drawbacks: (1) the number of SORs scale linearly with respect to the number N_{cfg} of CFGs in P but scale quadratically with respect to the number N_e of correlated electrons, such that both the consumption of memory and the repeated update of the SORs (which is necessary during the iterative selection) are unfavorable when N_e is large. (2) There may exist numerous redundant residues that do not provide any connection information, especially in the presence of many doubly occupied orbitals. (3) More seriously, the CFGs connected to a given CFG may be scattered widely in location, such that it is not easy to construct the Hamiltonian matrix in CSR format for efficient matrix-vector multiplications (unless a sorting step is taken but which itself is not cheap). It turns out that all these issues can be resolved by going to a particle-hole representation of the CFGs in P . The holes and particles are just the doubly occupied and the remaining singly or zero occupied orbitals in the common reference CFG $|R\rangle$ (which is already adopted in Eq. (17)), respectively. Then, the array `OrbOccBinary` representing a CFG can be decomposed into a hole (`HoleStr`) and a particle part (`PartStr`), such that connections between CFG pairs can be identified from those between `HoleStr`'s and between `PartStr`'s. To this end, we first define single transitions within the hole or particle orbitals as single inner excitations (SIE), whereas those between the two sets as single outer excitations (SOE) or de-excitations (SDE). While SIEs do not change the lengths of `HoleStr` and `PartStr`, a SOE (SDE) will increase (decrease) their lengths by one. Two `HoleStr`'s (`PartStr`'s) are connected only if their lengths differ less than three. A given `HoleStr/PartStr StrA` with length len can be connected with a `HoleStr/PartStr StrB` in eight possible ways,

1. StrB with length $len+2$ and two SOEs;
2. StrB with length $len+1$ and one SOE;
3. StrB with length $len+1$, one SIE and SOE;
4. StrB with length len and one SIE;
5. StrB with length len and two SIE;
6. StrB with length $len-1$ and one SDE;
7. StrB with length $len-1$, one SIE and one SDE;
8. StrB with length $len-2$ and two SDEs,

in addition to the case (denoted as 0) when StrB is identical with StrA.

The data structure of HoleStr is very simple. It consists of three parts: (1) an array of 64-bit integers recording the corresponding HoleStr; (2) eight hole connection arrays \mathcal{C}_{ph} recording the above connections to other HoleStr's; (3) one CFG array \mathcal{G}_{ph} recording the indices of CFGs sharing the same HoleStr. The data structure of PartStr is exactly the same. The connections between CFG pairs can then be identified in a simple way, since singly connected CFG pairs can only be one of the three single-connection types (SCT) $\{(2,2), (4,0), (6,6)\}$, whereas doubly connected CFG pairs can only be one of the eight double-connection types (DCT) $\{(1,1), (2,3), (3,2), (4,4), (5,0), (6,7), (7,6), (8,8)\}$. For instance, for a given CFG $|I\rangle$ with HoleStr HoleI and PartStr PartI, one can first find all HoleJ's and PartJ's according to the SCTs. Then, for each pair of HoleJ and PartJ, the intersection of their \mathcal{G}_{ph} 's contains all the CFGs that are singly connected to CFG $|I\rangle$. The doubly connected CFG pairs can be identified in the same way.

The Hamiltonian matrix can be constructed as follows: (A) loop over all CFGs $|I\rangle \in P$. (B) For each $|I\rangle$, find all CFGs $|J\rangle \in P$ connected with $|I\rangle$ but with indices smaller than that of $|I\rangle$. (C) Loop over $|J\rangle$ and calculate the Hamiltonian matrix elements between $|I\mu\rangle$

and $|J\nu\rangle$, which can readily be compressed in CSR format because the indices are now contiguous. As for the update of the Hamiltonian matrix, suppose that the old and new CSF spaces are $P_1 \subset P_2$ and P_2 , respectively, and the CSFs in $P_2 - P_1$ have been grouped according to their CFGs. After updating the connections between HoleStr's and between PartStr's, just loop over all newly added CFGs $|I\rangle$ in $P_2 - P_1$ and do (B) and (C) above.

In summary, as far as the handling of the P space is concerned, the present particle-hole algorithm is advantageous over the residue-based algorithm^{62,63,92} in several aspects, especially when N_e is large. First of all, the metadata of the HoleStr's and PartStr's is much smaller in size than that of the FORs and SORs, which is reflected by the much reduced memory consumption. For instance, for a variational space with 1164710 unique CFGs or 3059395 CSFs in the all-electron calculation of Cr_2 with the Ahlrichs SV basis set,⁹⁵ the memory cost of the HoleStr's and PartStr's is only 0.55 GB, whereas those of the FORs and SORs are 2.48 GB and 29.1 GB, respectively. Secondly, the simple structure of the HoleStr's and PartStr's allows for an easy construction of the Hamiltonian matrix in CSR format. For the case of Cr_2 , the Hamiltonian construction is speeded up by $2.5\times$. Thirdly, the connections between HoleStr's and between PartStr's can readily be reutilized. For example, when updating the Hamiltonian matrix from P_1 to P_2 mentioned previously, if some CSFs of a CFG in $P_2 - P_1$ are present in P_1 , the connections of this CFG to other CFGs in P_1 have already been encoded in the connections between HoleStrs and between PartStrs of P_1 . More interestingly, such connections can also be shared by CSF spaces of different spatial and/or spin symmetries, which facilitates the simultaneous calculation of several states of different spatial and/or spin symmetries with a common set of orthonormal orbitals.

As a final note, it deserves to be mentioned that, because of the random nature of the P space, the number of CFG pairs therein sharing the same Rot_Code is usually very small, such that the reutilization of BCCs is ineffective: it cannot compensate the overhead necessary for sorting the CFG pairs (which requires both substantial memory and

synchronous operations). Instead, recalculating the BCCs whenever needed turns out to be more efficient. However, the situation is different for the PT2 step, where the reutilization of BCCs by TUGA is essential.

6 Constraint-Based ENPT2

As long as the selectively determined variational space P and hence the zeroth-order eigenpairs $\{E_k^{(0)}, |\Psi_k^{(0)}\rangle\}$ are good enough, the remaining dynamic correlation can be accounted for accurately at the lowest level of theory. Here, we adopt the state-specific ENPT2

$$E_{c,k}^{(2)} = \sum_{|I\mu\rangle \in Q} \frac{|\langle I\mu | H | \Psi_k^{(0)} \rangle|^2}{E_k^{(0)} - H_{\mu\mu}^{II}} \quad (32)$$

$$= \sum_{|I\mu\rangle \in Q} \frac{\left| \sum_{|J\nu\rangle \in P} H_{\mu\nu}^{IJ} C_{\nu,k}^J \right|^2}{E_k^{(0)} - H_{\mu\mu}^{II}}. \quad (33)$$

Before evaluating this energy expression, several important points should be observed. Firstly, what the interaction really does is to excite one or two electrons from space P to space Q in all possible ways, leaving $N_e - 1$ or $N_e - 2$ CFGs in P , which are nothing but the respective FORs and SORs mentioned in the previous section. Reversely, the excited CFGs can be generated by inserting one and two electrons into the FORs and SORs, respectively. Therefore, the FORs and SORs provide natural connections between the two spaces and are hence the proper organizing units. Secondly, the number of CFG pairs sharing the same Rot_Code can be very large, such that is essential to reutilize the BCCs by TUGA. Thirdly, the summation over $|I\mu\rangle \in Q$ can be extended to include also the CSFs in P , by

precomputing and finally subtracting their PT2-like energy $\bar{E}_{c,k}^{(2)}$,⁶³ viz.,

$$E_{c,k}^{(2)} = \tilde{E}_{c,k}^{(2)} - \bar{E}_{c,k}^{(2)}, \quad (34)$$

$$\tilde{E}_{c,k}^{(2)} = \sum_{|I\mu\rangle \in W} \frac{\left| \sum_{|J\nu\rangle \in P, |J\nu\rangle \neq |I\mu\rangle} H_{\mu\nu}^{IJ} C_{\nu,k}^J \right|^2}{E_k^{(0)} - H_{\mu\mu}^{II}}, \quad W = P \cup Q, \quad (35)$$

$$\bar{E}_{c,k}^{(2)} = \sum_{|I\mu\rangle \in P} \frac{\left| \langle I\mu | H | \Psi_k^{(0)} \rangle - C_{\mu,k}^I H_{\mu\mu}^{II} \right|^2}{E_k^{(0)} - H_{\mu\mu}^{II}} \quad (36)$$

$$= \sum_{|I\mu\rangle \in P} (C_{\mu,i}^I)^2 (E_i^{(0)} - H_{\mu\mu}^{II}), \quad (37)$$

where use of the relation $\langle I\mu | H | \Psi_k^{(0)} \rangle = C_{\mu,k}^I E_k^{(0)}$ has been made when going from Eq. (36) to Eq. (37). The negative term in the numerator of Eq. (36) arises from the fact that the diagonal terms have been excluded in Eq. (35). This way, there is no need to double check whether the excited CSFs belong to Q or P , which is every expensive. Fourthly, since there is no coupling between the $|I\mu\rangle$ functions, the whole W space can be decomposed into a series of disjoint subspaces $\{W_i\}_i^{N_s}$, so as to reduce memory requirement and meanwhile facilitate the parallelization.

Following the idea of constraint PT2,⁶³ a CFG subspace W_i of W can be defined by a constraint consisting of L_c highest occupied orbitals (say, p_1, p_2, \dots, p_{L_c} in ascending order) as well as their occupation numbers (say, $n_{p_1}, n_{p_2}, \dots, n_{p_{L_c}}$). The number N_s of such subspaces is bounded by $C_{N_{orb}}^{L_c} \times 2^{L_c}$. To achieve this, the FORs and SORs of P are first generated and sorted, with the unique ones recorded in arrays \mathcal{R}_1 and \mathcal{R}_2 , respectively. Here, each unique residue is associated with an array of records $\{indx, orbj, orbl\}$ to trace how it arises: *indx* records the CFG in P , whereas *orbj* and *orbl* record the orbitals from which electrons are removed (i.e., the j and l indices of $e_{ij,kl}$). Note that *orbj* can be equal to *orbl* for a SOR, whereas only *orbsj* is needed for a FOR. Then, those FORs and SORs that can generate the CFGs belonging to W_i must be identified. Since the occupation pattern of a CFG in W_i must be $(0, \dots, 0, n_{p_{L_c}}, 0, \dots, 0, n_{p_{L_c-1}}, 0, \dots, 0, n_{p_1})$ for orbitals of

indices not smaller than p_1 , a valid residue with occupation numbers $\{m_n\}_{n=0}^{N_{orb}-1}$ must be subject to the restrictions $m_p \leq n_p$ for $p \geq p_1$ and $R_t = \sum_{p=p_1}^{N_{orb}-1} (n_p - m_p) \in [0, 2]$. For the case of FORs, R_t can be either 0 or 1, which are labeled c1 and c2, respectively. For the former, $n_p = m_p$ for all $p \geq p_1$. For the latter, there exists one orbital q such that $n_q = m_q + 1$ for $q \in [p_1, p_{L_c}]$ and $n_p = m_p$ for $p \geq p_1$ other than q . For the case of SORs, R_t can also be 2, which leads to two additional conditions: (a) c3: if there exists $q \geq p_1$ with $n_q = 2$ and $m_q = 0$, then $n_p = m_p$ for $p \geq p_1$ other than q . (b) c4: if there exist q and r with $n_q - m_q = 1$ and $n_r - m_r = 1$, then $n_p = m_p$ for $p \geq p_1$ other than q and r . The valid FORs and SORs can be classified according to their occupation patterns for orbitals $p \geq p_1$, such that those of the same occupation pattern are located contiguously in $\mathcal{R}_1/\mathcal{R}_2$, thereby forming a segment. The numbers of such patterns/segments are $1 + C_{L_c}^1$ for FORs (1 for c1 and $C_{L_c}^1$ for c2) and $1 + C_{L_c}^1 + C_{L_c}^1 + C_{L_c}^2$ for SORs ($C_{L_c}^1$ for c3 and $C_{L_c}^2$ for c4). The head R_{min} (tail R_{max}) of a segment is determined by distributing the remaining $N_e - \sum_{p \geq p_1}^{N_{orb}-1} m_p - N_R$ electrons ($N_R = 1$ for FORs and 2 for SORs) to orbitals as close to (far away from) p_1 as possible. They can be used to locate the relevant residues by binary search of the segments. For a given residue, each way of adding electrons will generate a CFG $|I\rangle \in W_i$, whose connections with the CFGs $\{|J\rangle\}$ in P can be established by looping over the records $\{indx, orbj, orbl\}$ associated with the residue (NB: each $indx$ corresponds to a CFG $|J\rangle$). Such pair connection records (PCR) are stored in array \mathcal{C}_{IJ} , which is to be sorted to group those records sharing the same $|I\rangle$ together. Note in passing that in principle only the SORs are needed to generate such PCRs. However, very many duplicate singly connected CFG pairs can be generated from the SORs and the removal of them can be very costly. Instead, it is more favorable to take the (non-duplicate) singly connected CFG pairs from the FORs and simply dump the ones from the SORs. The price to pay is just some extra memory. For a given PCR, an interaction record $\{ROT_Code, I, J, integrals\}$ is further needed to calculate $\sum_{\nu} \langle I\mu | H | J\nu \rangle C_{\nu,k}^J$ for all CSFs of $|I\rangle \in W_i$. It can be constructed by first identifying the ROT for (I, J) and then

fetching the integrals based on ROT_Orb. All the interaction records are stored in array \mathcal{V}_{IJ} , which is to be sorted according to ROT_Code to reuse the BCCs by TUGA.

At this moment two key factors should be observed: (1) the sizes of different subspaces W_i may differ by orders of magnitude, which renders the load in parallelization extremely imbalanced on one hand and the reutilization of BCCs of very small subspaces virtually impossible. (2) Both the generation and sorting of the connection and interaction data can be very expensive. The former can be resolved by precomputing the sizes of subspaces, so as to merge small subspaces together or further split very large subspaces into smaller ones. Although not very cheap, the expense of this null step is overcompensated by the gain in parallelization efficiency. As for the latter, the red-black tree-based algorithm adopted in our previous implementation⁶⁶ turns out to be inefficient: too much time is wasted on the searching and insertion, due to the fact that the nodes in red-black trees are scattered in memory, thereby resulting in a very low cache-hit rate. Since array appending and sorting are more efficient than tree insertion and searching, we here employ arrays instead of trees for the data. What is essential is then how to impose a particular structure to the array of raw data, according to which a possibly optimal sorting algorithm can be found. For instance, if the array occurs automatically as sorted subarrays with an equal length, the Timsort algorithm^{77,78} would be the best choice (NB: Timsort appears to work well even if some subarrays have different lengths). To this end, the above connection array \mathcal{C}_{IJ} is to be generated as follows: (1) for the c2 segment of FORs or the c3 and c4 segments of SORs, the electron-accepting orbitals are already fixed and are the same for all the residues within the segment. Since the FORs and SORs are already sorted, the PCRs generated from such segment are automatically sorted. (2) For the c1 segment of FORs or the c2 segment of SORs, one electron should be added to orbital $s \in [0, p_1 - 1]$. If the loop over s proceeds in descending order, the generated CFGs will be in ascending order, leading to ordered PCRs for each residue. Therefore, the PCRs for such segment consist of several ordered subarrays, thereby well suited for the Tim-

sort algorithm. (3) For the c1 segment of SORs, two electrons should be added to orbitals $i, k \in [0, p_1 - 1]$ with $k \geq i$ (NB: i, k are the indices of $e_{ij,kl}$). If the outer loop over k and the inner loop over i for each k both proceed in descending order, the PCRs will be of the same structure as case (2) and hence fit the Timsort algorithm as well. After looping over all residue segments, the whole C_{IJ} array will consist of several sorted subarrays and can finally be sorted by Timsort. In contrast, the interaction array \mathcal{V}_{IJ} cannot be prepared in any particular structure and is hence sorted simply by `std::sort()` in C++.

The efficacy of the above PT2 algorithm can quickly be revealed by again taking Cr_2/SV as an example. It turns out that the smaller the C_{min} (i.e., the larger the variational space P), the larger the speedup of PT2 over the previous, red-black tree-based implementation,⁶⁶ amounting to $21\times$ for P with 1.1M CSFs. If desired, two additional cutoffs can be employed for the PT2 correction: (1) those doubly excited CFGs $|I\rangle$ with $\tilde{H}^{IJ} \max_{\nu} |C_{\nu,k}^J|$ smaller than a threshold (e.g., $10^{-3}C_{min}$) can be neglected. (2) Those CSFs $|I\mu\rangle$ with $|\langle I\mu|H|\Psi_k^{(0)}\rangle|$ smaller than a threshold (e.g., 5×10^{-9}) can further be neglected.

7 Results and discussion

All the calculations were performed with the BDF program package^{96–100} on one node with 4 Intel(R) Xeon(R) Gold 6240 CPUs (in total 72 physical cores) and 768 GB memory.

7.1 Comparison of different ranking criteria

The very first point to be checked is the compactness of the final variational space P determined by different ranking criteria discussed in Sec. 4. To this end, all-electron non-relativistic calculations were performed on the ground state of Cr_2 with the Ahlrichs SV basis set⁹⁵ at two interatomic distances, R_{eq} ($=1.68 \text{ \AA}$) and $2.0R_{eq}$. It can be seen from Fig. 3 that, as the most rigorous ranking criterion, CIPSI (24) does lead to the smallest number of CSFs and hence the most compact wave function for the same variational energy (NB:

although not documented here, the original iCI criterion (26)/(27) is virtually identical with CIPSI (24)). It appears that HBCI (30)/(31) follows closely CIPSI. However, as can be seen from Fig. 4, this arises with a high price: the variational space P_1 determined by HBCI (30)/(31) is actually very large and is only reduced (by a factor of more than 10!) by the pruning step. That is, the HBCI ranking criterion is too loose, thereby bringing in too many unimportant CSFs, more than 90% of which are pruned away. This is clearly a waste of time for Hamiltonian construction and diagonalization. Note in passing that the HBCI ranking used here is different from the original one,⁵⁰ which does not invoke any pruning. It is also clear that the iCI criterion (28)/(29) leads to the least compact variational space P among the three considered ranking criteria. However, the situation gets improved steadily by reducing C_{min} . More importantly, the iCI selection is much more efficient than the other two (cf. Fig. 5): the cost of the iCI selection is only 20% of that of PT2, whereas the other two are approximately two times more expensive than their PT2's. Therefore, the slight loss of compactness is overcompensated by the gain in efficiency. An additional point deserves to be mentioned here: while typically less than 1% of the CSFs in the CIPSI and iCI variational spaces have coefficients somewhat smaller in absolute value than C_{min} , such CSFs can be up to 10% in the pruned HBCI variational space.

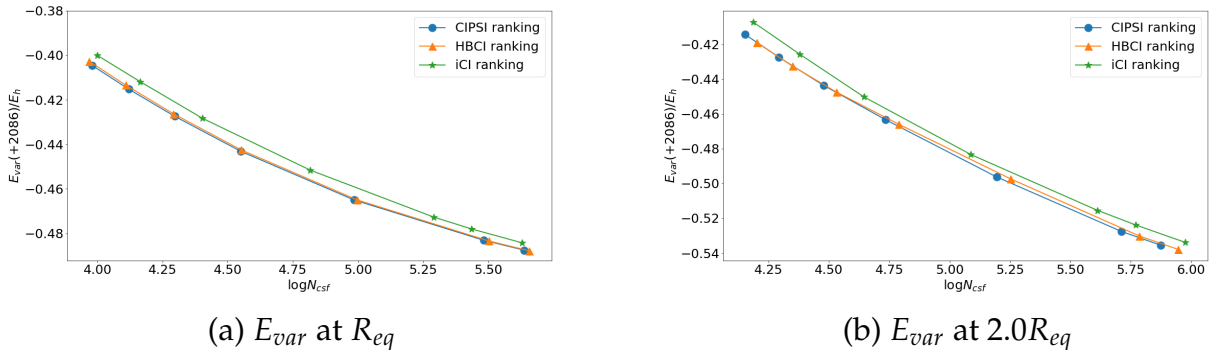


Figure 3: The all-electron variational energy E_{var} of Cr_2/SV as function of the number N_{csf} of CSFs selected by the CIPSI (24), iCI (28)/(29) and HBCI (30)/(31) ranking criteria.

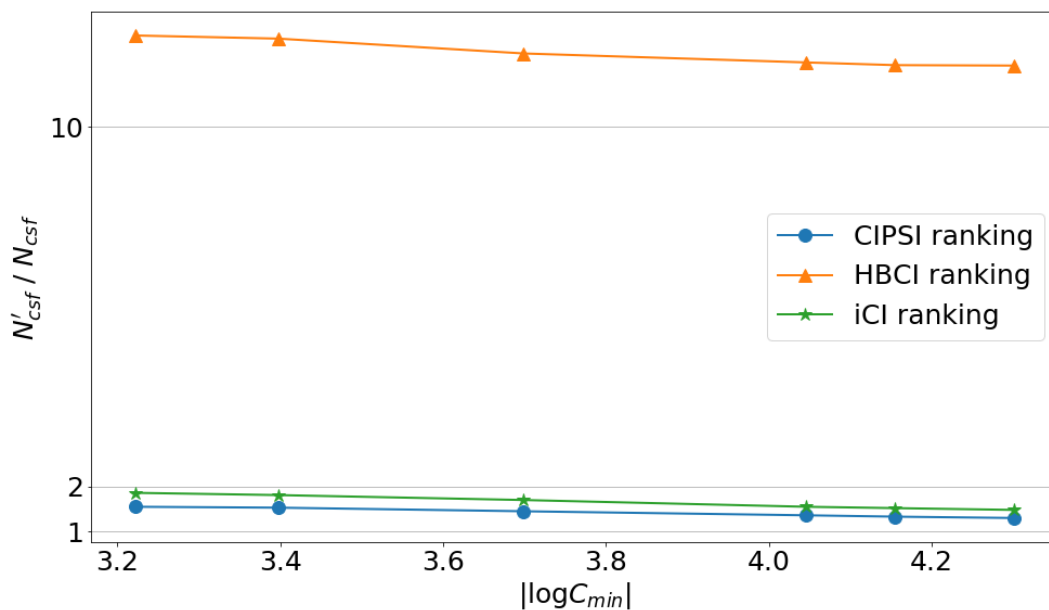


Figure 4: The size ratio N'_{csf}/N_{csf} between the unpruned and pruned variational spaces determined by the CIPSI (24), iCI (28)/(29) and HBCI (30)/(31) ranking criteria.

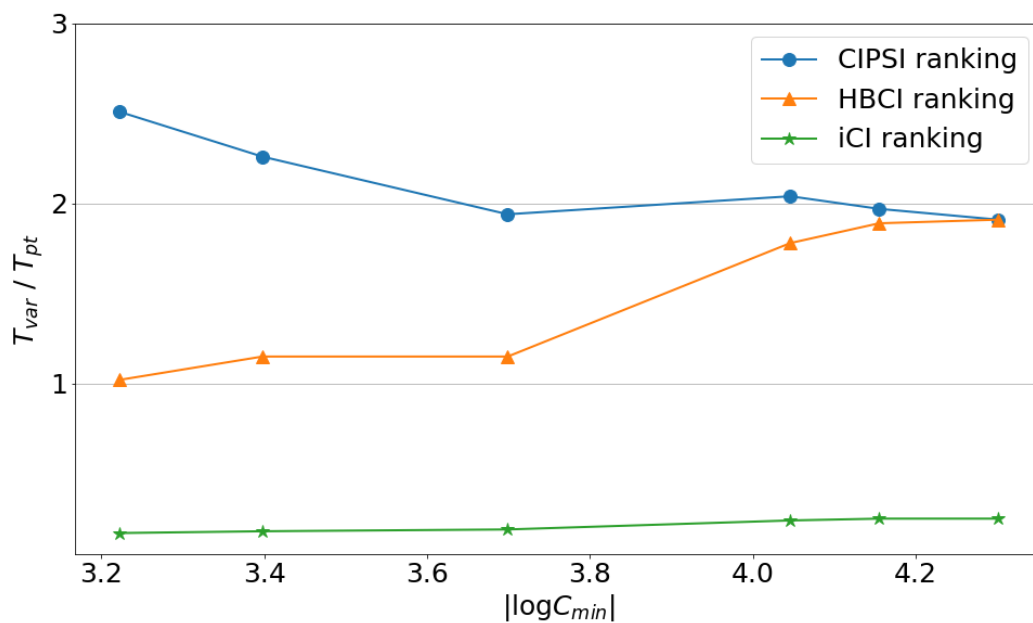


Figure 5: The time ratio T_{var}/T_{pt} between selection and PT2 by the CIPSI (24), iCI (28)/(29) and HBCI (30)/(31) ranking criteria.

7.2 Cr₂

Given the improved efficiency of iCIPT2, we are now ready to perform more accurate calculations on the ground state of Cr₂, a classic strongly correlated system for testing various methods.^{18,51,62,63,94,101–103} To this end, the spin-free exact two-component (sf-X2C) relativistic Hamiltonian^{104,105} and the cc-pVDZ-DK basis¹⁰⁶ were adopted, along with an active space of (28e, 76o) that is composed of 4.8×10^{27} CSFs. While the Ne-core orbitals are just HF orbitals, the NOs were used for correlation, which were generated in two ways, (A) ‘partially dynamic’ (see point (4) in the end of Sec. 4) and (B) ‘static’. In the latter, the NOs were generated with $C_{min} = 1.0 \times 10^{-4}$ and then used for all smaller C_{min} ’s. In this case, the variational space determined at a C_{min} can directly be used as initial guess for a smaller C_{min} . The results with the two sets of NOs are documented in Tables 5 and 6, respectively. It is of interest to see that the extrapolated value ($-2099.9223(4) E_h$) by scheme B is very close to the HBCI value ($-2099.9224(6) E_h$).¹⁰² However, it is believed that the extrapolated value ($-2099.9240(2) E_h$) by scheme A is more accurate (by $-1.7 mE_h$) than that by scheme (B) because the partially dynamically generated NOs in the former are of better quality than the fixed ones in the latter. It is for sure that the two sets of calculations would agree with each other completely by further reducing C_{min} , so as to sample even larger portions of the full Hilbert space and hence minimize orbital rotation effects. For instance, in the all-electron nonrelativistic calculations on Cr₂ with the SV basis, the difference between the energies by scheme A ($-2086.44468(2) E_h$) and scheme B ($-2086.44466(2) E_h$) is only $-0.02 mE_h$. Here, the largest FOIS (1.3×10^{11}) sampled by iCIPT2/SV is ca. $10^{-8}\%$ of the full space (1.4×10^{21}). In contrast, the largest FOIS (3.2×10^{12}) sampled by sf-X2C-iCIPT2/cc-pVDZ-DK is only $10^{-14}\%$ of the full space (4.8×10^{27}).

Table 5: Frozen-core sf-X2C-iCIPT2/cc-pVDZ-DK calculations of the ground state of Cr_2 at $R_{eq} = 1.68 \text{ \AA}$ ^a

C_{\min}^b	N_{cfg}^c	N_{csf}^d	\tilde{N}_{csf}^e	\tilde{N}_{det}^f	$E_{var}(+2099)/E_h$	$E_{tot}(+2099)/E_h$	T_{wall}/s
5.0×10^{-5}	455404	3136853	896527	3666946	-0.81095	-0.90466	464
4.0×10^{-5}	615595	4512684	1250882	5197093	-0.81929	-0.90612	641
3.0×10^{-5}	903347	7115256	1904606	8059852	-0.82909	-0.90785	973
2.0×10^{-5}	1560133	13369034	3470331	15033913	-0.84161	-0.90100	1775
1.5×10^{-5}	2281773	20737948	5268475	23176915	-0.84926	-0.91128	2765
1.0×10^{-5}	3959566	38959372	9616690	43154698	-0.85945	-0.91300	5194
9.0×10^{-6}	4565597	45851900	11235054	50662572	-0.86191	-0.91341	6309
0.0 ^g	-2099.9240±0.0002						

^a D_{2h} symmetry; HF energy: $-2098.536329 E_h$; active space: (28e, 76o); partially dynamically generated NOs (see point (4) in the end of Sec. 4).

^b Threshold for pruning CSF in the variational (var) space.

^c Number of orbital configurations in the variational space.

^d Number of CSFs corresponding to N_{cfg} .

^e Number of CSFs after selection, among which about 0.5% have coefficients slightly smaller in absolute values than C_{\min} (which is due to a final diagonalization).

^f Estimated number of determinants according to the expression $\sum_I \frac{\tilde{N}_{csf}^I}{N_{csf}^I} N_{det}^I$, with N_{det}^I being the numbers of determinants of CFG $|I\rangle$.

^g Extrapolated value by linear fit of the E_{total} vs. $|E_c^{(2)}|$ plot, with uncertainty being half the length of 95% confidence interval.

Table 6: Frozen-core sf-X2C-iCIPT2/cc-pVDZ-DK calculations of the ground state of Cr_2 at $R_{eq} = 1.68 \text{ \AA}$ ^a

C_{\min}	N_{cfg}	N_{csf}	\tilde{N}_{csf}	\tilde{N}_{det}	$E_{var}(+2099)/E_h$	$E_{tot}(+2099)/E_h$	T_{wall}/s
5.0×10^{-5}	425431	2892927	840568	3438022	-0.809883	-0.903447	434
4.0×10^{-5}	573307	4145556	1168810	4857157	-0.818110	-0.904792	599
3.0×10^{-5}	840891	6513720	1779100	7530355	-0.827922	-0.906404	916
2.0×10^{-5}	1449299	12182405	3233090	14006309	-0.840470	-0.908481	1651
1.5×10^{-5}	2153481	19286806	4989382	21922383	-0.847846	-0.909859	2645
1.0×10^{-5}	3716908	35893887	9034413	40531897	-0.858790	-0.911610	4978
9.0×10^{-6}	4284579	42309173	10542471	47528961	-0.861208	-0.912028	5608
0.0	-2099.9223±0.0004						
0.0 ^b	-2099.9224±0.0006						
0.0 ^c	-2099.9195±0.0027						

^a Fixed NOs generated with $C_{min} = 1.0 \times 10^{-4}$. For additional explanations see Table 5.

^b HBCI.¹⁰²

^c DMRG ($M = 16000$).¹⁰³

7.3 [2Fe-2S]

As a final example, we consider $[\text{Fe}_2\text{S}_2(\text{SCH}_3)_4]^{2-}$ (abbreviated as [2Fe-2S]). Albeit a simplest system for modeling iron-containing enzymes,¹⁹ even the minimal chemically meaningful active space (30e, 20o) already contains 240374016 CSFs (52581816, 99419400, 64438500, 20575100, 3174444, and 184756 CSFs for spins from 0 to 5, respectively). The 20 active orbitals here include Fe $3d$ and S $3p$ of the core [2Fe-2S] as well as their four σ -bonds with ligands. To make a direct comparison with the previous work, the (nonrelativistic) molecular orbital integrals are taken simply from Ref. 19. The extrapolated (valence) energy of the singlet ground state is $-116.60574(6) E_h$ (cf. Table 7), very close to the DMRG value of $-116.60561 E_h$ with $M = 8000$.¹⁰⁷ It is more appealing to take a closer look at the wave function (selected with $C_{min} = 5.0 \times 10^{-6}$): it is composed of 41.13% Fe(II) – Fe(II), 22.69% Fe(III) – Fe(II), 22.01% Fe(II) – Fe(I), 6.05% Fe(III) – Fe(I), 3.40% Fe(III) – Fe(III), and 2.86% Fe(I) – Fe(I), but the leading CSF has a weight only of 3.36% and stems from Fe(III) – Fe(III) instead of the leading structure Fe(II) – Fe(II). It is not clear whether this peculiar picture will hold for a larger active space, especially in conjunction with localized orbitals. Nevertheless, it is perfectly legitimate to further calculate more spin states, just to reveal the efficacy of iCIPT2.

Although the particle-hole algorithm presented in Sec. 5 allows for simultaneous calculations of several states of different spins with a common set of orbitals, the function is not yet at our disposal. Instead, states of different spins are calculated here separately. One then has to face the issue that the quality of states of different spins may be different for the same C_{min} , so as to affect the relative energies. To circumvent this problem, we decompose the vertical excitation energy $\Delta E_{S,i} (= E_{S,i} - E_{0,0})$ of state i with spin S into two terms, $\Delta E_{S,i} - \Delta E_{S,0}$ and $\Delta E_{S,0} - \Delta E_{0,0}$. The former is calculated with the same C_{min} , whereas the latter is set to the extrapolated value, i.e.,

$$\Delta E_{S,i}(0.0) = [E_{S,i}(C_{min}) - E_{S,0}(C_{min})] + [E_{S,0}(0.0) - E_{0,0}(0.0)]. \quad (38)$$

In essence, what is assumed here is that different states of the same spin have the same extrapolation distance. The so-calculated excitation energies for all states below 1.8 eV are documented in Table 8 and further plotted in Fig. 6. Interestingly, the lowest 6 states originate just from the lowest state of each of the 6 possible spins $S \in [0, 5]$ that result from the coupling of the two high-spin- $\frac{5}{2}$ ionic configurations Fe(III) $3d^5$ and are energetically ordered in increasing spin. However, the remaining 30 states of different spins are intersected within an interval of 0.91 eV. That is, they are separated in average by only 0.03 eV, just like the gap between the lowest singlet and triplet states. It is clear that such complicated spin structure cannot be handled by determinant-based methods due to severe spin contaminations.

Table 7: The singlet ground state of $[\text{Fe}_2\text{S}_2(\text{SCH}_3)_4]^{2-}$ (for additional explanations see Table 5)

C_{\min}	N_{cfg}	N_{csf}	\tilde{N}_{csf}	\tilde{N}_{det}	E_{var}/E_h	E_{tot}/mE_h
2.0×10^{-5}	313428	6242941	568382	3056319	-116.602301	-116.604325
1.5×10^{-5}	396163	7436740	754898	4031212	-116.603153	-116.604691
1.0×10^{-5}	540358	9332213	1108867	5866360	-116.604010	-116.605046
9.0×10^{-6}	586437	9908183	1228988	6485715	-116.604196	-116.605120
7.0×10^{-6}	744932	11779934	1673904	8765188	-116.604554	-116.605256
5.0×10^{-6}	938275	13485301	2236247	11619598	-116.604908	-116.605385
0.0					-116.60574 \pm 0.00006	

8 Conclusions and Outlook

Sticking to the parlance of static and dynamic correlations, there could be two paradigms for handling strongly correlated systems of electrons, viz. “more static, less dynamic” and “less static, more dynamic”. It is the former that is followed by the family of sCI+PT2 methods, among which iCIPT2 stands out in several aspects as already highlighted in the Introduction. Its efficiency has been improved herein by up to 20 \times via three major techniques: a new criterion for configuration selection, a new particle-hole algorithm for Hamiltonian construction, and a new data structure for the quick sorting of the FOIS, in

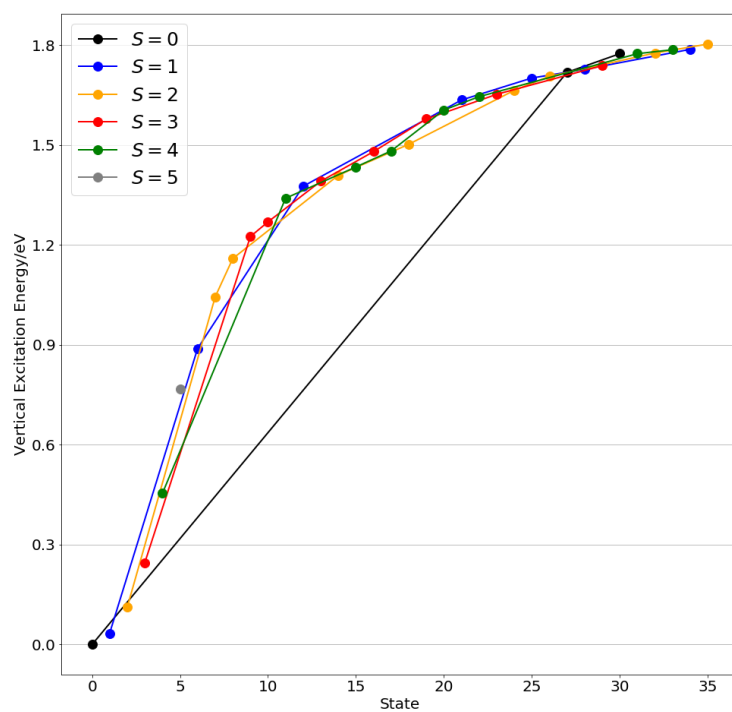


Figure 6: Vertical excitation energies of low-lying excited states of [2Fe-2S]

Table 8: Vertical excitation energies (ΔE in eV) of low-lying excited states of [2Fe-2S]

State	$2S + 1$	ΔE	State	$2S + 1$	ΔE
0	1	0.000	18	5	1.502
1	3	0.034	19	7	1.578
2	5	0.112	20	9	1.605
3	7	0.246	21	3	1.635
4	9	0.454	22	9	1.645
5	11	0.767	23	7	1.652
6	3	0.889	24	5	1.664
7	5	1.044	25	3	1.701
8	5	1.159	26	5	1.706
9	7	1.225	27	1	1.718
10	7	1.269	28	3	1.727
11	9	1.340	29	7	1.738
12	3	1.376	30	1	1.774
13	7	1.391	31	9	1.774
14	5	1.409	32	5	1.776
15	9	1.434	33	9	1.786
16	7	1.480	34	3	1.787
17	9	1.482	35	5	1.803

addition to the workhorse TUGA for computing and reutilizing the basic coupling coefficients between randomly selected CSFs. All these can be applied to other types of sCI+PT2 as well. As revealed by several examples, iCIPT2 can indeed be characterized as a near-exact approach. However, it is still memory intensive, even though the FOIS has been decomposed into disjoint subspaces. A possible way to resolve this issue is to evaluate the PT2 correction in a stochastic manner. Other immediate extensions of iCIPT2 include simultaneous treatment of states of different spatial and/or spin symmetries (which is furnished by the particle-hole algorithm), perturbative treatment of spin-orbit couplings (via the sf-X2C+soc-DKH1 Hamiltonian^{104,105}), and direct access of high-lying states of a given energy window (which is furnished by the iVI eigensolver^{83,85}), etc. Work along these directions are being undertaken at our laboratory.

Acknowledgement

The research of this work was supported by National Natural Science Foundation of China (Grant Nos. 21833001 and 21973054) and the North Dakota University System.

References

- (1) Liu, W. Essentials of relativistic quantum chemistry. *J. Chem. Phys.* **2020**, *152*, 180901.
- (2) Liu, W. Relativistic quantum chemistry: today and tomorrow. *Sci. Sin. Chim.* **2020**, DOI: 10.1360/SSC-2020-0120.
- (3) Chaudhuri, R. K.; Freed, K. F.; Hose, G.; Piecuch, P.; Kowalski, K.; Włoch, M.; Chattopadhyay, S.; Mukherjee, D.; Rolik, Z.; Szabados, Á.; Tóth, G.; Surján, P. R. Comparison of low-order multireference many-body perturbation theories. *J. Chem. Phys.* **2005**, *122*, 134105.
- (4) Hoffmann, M. R.; Datta, D.; Das, S.; Mukherjee, D.; Szabados, Á.; Rolik, Z.; Surján, P. R. Comparative study of multireference perturbative theories for ground and excited states. *J. Chem. Phys.* **2009**, *131*, 204104.
- (5) Lyakh, D. I.; Musiaż, M.; Lotrich, V. F.; Bartlett, R. J. Multireference nature of chemistry: The coupled-cluster view. *Chem. Rev.* **2012**, *112*, 182–243.
- (6) Sherrill, C. D.; Schaefer III, H. F. The configuration interaction method: Advances in highly correlated approaches. *Adv. Quantum Chem.* **1999**, *34*, 143–269.
- (7) Szalay, P. G.; Muller, T.; Gidofalvi, G.; Lischka, H.; Shepard, R. Multiconfiguration self-consistent field and multireference configuration interaction methods and applications. *Chem. Rev.* **2012**, *112*, 108–181.

- (8) Lischka, H.; Nachtigallova, D.; Aquino, A. J.; Szalay, P. G.; Plasser, F.; Machado, F. B.; Barbatti, M. Multireference approaches for excited states of molecules. *Chem. Rev.* **2018**, *118*, 7293–7361.
- (9) Liu, W.; Hoffmann, M. R. iCI: Iterative CI toward full CI. *J. Chem. Theory Comput.* **2016**, *12*, 1169–1178, (E) **2016**, *12*, 3000.
- (10) White, S. R. Density matrix formulation for quantum renormalization groups. *Phys. Rev. Lett.* **1992**, *69*, 2863.
- (11) White, S. R. Density-matrix algorithms for quantum renormalization groups. *Phys. Rev. B* **1993**, *48*, 10345–10356.
- (12) White, S. R.; Martin, R. L. Ab initio quantum chemistry using the density matrix renormalization group. *J. Chem. Phys.* **1999**, *110*, 4127–4130.
- (13) Mitrushenkov, A. O.; Fano, G.; Ortolani, F.; Linguerri, R.; Palmieri, P. Quantum chemistry using the density matrix renormalization group. *J. Chem. Phys.* **2001**, *115*, 6815–6821.
- (14) Chan, G. K.-L.; Head-Gordon, M. Highly correlated calculations with a polynomial cost algorithm: A study of the density matrix renormalization group. *J. Chem. Phys.* **2002**, *116*, 4462–4476.
- (15) Chan, G. K.-L.; Sharma, S. The density matrix renormalization group in quantum chemistry. *Annu. Rev. Phys. Chem.* **2011**, *62*, 465–481.
- (16) Sharma, S.; Chan, G. K.-L. Spin-adapted density matrix renormalization group algorithms for quantum chemistry. *J. Chem. Phys.* **2012**, *136*, 124121.
- (17) Wouters, S.; Van Neck, D. The density matrix renormalization group for ab initio quantum chemistry. *Eur. Phys. J. D* **2014**, *68*, 272.

- (18) Olivares-Amaya, R.; Hu, W.; Nakatani, N.; Sharma, S.; Yang, J.; Chan, G. K.-L. The ab-initio density matrix renormalization group in practice. *J. Chem. Phys.* **2015**, *142*, 034102.
- (19) Li, Z.; Chan, G. K.-L. Spin-Projected Matrix Product States: Versatile Tool for Strongly Correlated Systems. *J. Chem. Theory Comput.* **2017**, *13*, 2681–2695.
- (20) Baiardi, A.; Reiher, M. The density matrix renormalization group in chemistry and molecular physics: Recent developments and new challenges. *J. Chem. Phys.* **2020**, *152*, 040903.
- (21) Booth, G. H.; Thom, A. J. W.; Alavi, A. Fermion Monte Carlo without fixed nodes: A game of life, death, and annihilation in Slater determinant space. *J. Chem. Phys.* **2009**, *131*, 054106.
- (22) Cleland, D.; Booth, G. H.; Alavi, A. Communications: Survival of the fittest: Accelerating convergence in full configuration-interaction quantum Monte Carlo. *J. Chem. Phys.* **2010**, *132*, 041103.
- (23) Blunt, N.; Booth, G. H.; Alavi, A. Density matrices in full configuration interaction quantum Monte Carlo: Excited states, transition dipole moments, and parallel distribution. *J. Chem. Phys.* **2017**, *146*, 244105.
- (24) Petruzielo, F. R.; Holmes, A. A.; Changlani, H. J.; Nightingale, M. P.; Umrigar, C. J. Semistochastic projector monte carlo method. *Phys. Rev. Lett.* **2012**, *109*, 230201.
- (25) Holmes, A. A.; Changlani, H. J.; Umrigar, C. J. Efficient heat-bath sampling in Fock space. *J. Chem. Theory Comput.* **2016**, *12*, 1561–1571.
- (26) Ten-no, S. Stochastic determination of effective Hamiltonian for the full configuration interaction solution of quasi-degenerate electronic states. *J. Chem. Phys.* **2013**, *138*, 164126.

- (27) Ghanem, K.; Lozovoi, A. Y.; Alavi, A. Unbiasing the initiator approximation in full configuration interaction quantum Monte Carlo. *J. Chem. Phys.* **2019**, *151*, 224108.
- (28) Blunt, N. S. A hybrid approach to extending selected configuration interaction and full configuration interaction quantum Monte Carlo. *J. Chem. Phys.* **2019**, *151*, 174103.
- (29) Dobrautz, W.; Smart, S. D.; Alavi, A. Efficient formulation of full configuration interaction quantum Monte Carlo in a spin eigenbasis via the graphical unitary group approach. *J. Chem. Phys.* **2019**, *151*, 094104.
- (30) Neufeld, V. A.; Thom, A. J. Accelerating Convergence in Fock Space Quantum Monte Carlo Methods. *J. Chem. Theory Comput.* **2020**, *16*, 1503–1510.
- (31) Deustua, J. E.; Magoulas, I.; Shen, J.; Piecuch, P. Communication: Approaching exact quantum chemistry by cluster analysis of full configuration interaction quantum Monte Carlo wave functions. *J. Chem. Phys.* **2018**, *149*, 151101.
- (32) Lyakh, D. I.; Bartlett, R. J. An adaptive coupled-cluster theory:@CC approach. *J. Chem. Phys.* **2010**, *133*, 244112.
- (33) Xu, E.; Uejima, M.; Ten-no, S. L. Full Coupled-Cluster Reduction for Accurate Description of Strong Electron Correlation. *Phys. Rev. Lett.* **2018**, *121*, 113001.
- (34) Xu, E.; Uejima, M.; Ten-No, S. L. Towards near-exact solutions of molecular electronic structure: Full coupled-cluster reduction with a second-order perturbative correction. *J. Phys. Chem. Lett.* **2020**, *11*, 9775–9780.
- (35) Zhang, T.; Evangelista, F. A. A deterministic projector configuration interaction approach for the ground state of quantum many-body systems. *J. Chem. Theory Comput.* **2016**, *12*, 4326–4337.

- (36) Eriksen, J. J.; Lipparini, F.; Gauss, J. Virtual orbital many-body expansions: A possible route towards the full configuration interaction limit. *J. Phys. Chem. Lett.* **2017**, *8*, 4633–4639.
- (37) Eriksen, J. J.; Gauss, J. Many-Body Expanded Full Configuration Interaction. I. Weakly Correlated Regime. *J. Chem. Theory Comput.* **2018**, *14*, 5180–5191.
- (38) Eriksen, J. J.; Gauss, J. Many-Body Expanded Full Configuration Interaction. II. Strongly Correlated Regime. *J. Chem. Theory Comput.* **2019**, *15*, 4873–4884.
- (39) Eriksen, J. J.; Gauss, J. Generalized Many-Body Expanded Full Configuration Interaction Theory. *J. Phys. Chem. Lett.* **2019**, *10*, 7910–7915.
- (40) Zimmerman, P. M. Incremental full configuration interaction. *J. Chem. Phys.* **2017**, *146*, 104102.
- (41) Zimmerman, P. M. Strong correlation in incremental full configuration interaction. *J. Chem. Phys.* **2017**, *146*, 224104.
- (42) Fales, B. S.; Seritan, S.; Settje, N. F.; Levine, B. G.; Koch, H.; Martínez, T. J. Large-Scale Electron Correlation Calculations: Rank-Reduced Full Configuration Interaction. *J. Chem. Theory Comput.* **2018**, *14*, 4139–4150.
- (43) Greene, S. M.; Webber, R. J.; Weare, J.; Berkelbach, T. C. Beyond walkers in stochastic quantum chemistry: reducing error using fast randomized iteration. *J. Chem. Theory Comput.* **2019**, *15*, 4834–4850.
- (44) Bytautas, L.; Ruedenberg, K. Correlation energy extrapolation by intrinsic scaling. I. Method and application to the neon atom. *J. Chem. Phys.* **2004**, *121*, 10905–10918.
- (45) Bytautas, L.; Ruedenberg, K. Correlation energy extrapolation by intrinsic scaling. II. The water and the nitrogen molecule. *J. Chem. Phys.* **2004**, *121*, 10919–10934.

- (46) Greer, J. C. Monte Carlo configuration interaction. *J. Comput. Phys.* **1998**, *146*, 181–202.
- (47) Coe, J. P.; Paterson, M. J. Development of Monte Carlo configuration interaction: Natural orbitals and second-order perturbation theory. *J. Chem. Phys.* **2012**, *137*, 204108.
- (48) Ohtsuka, Y.; Hasegawa, J.-y. Selected configuration interaction method using sampled first-order corrections to wave functions. *J. Chem. Phys.* **2017**, *147*, 034102.
- (49) Coe, J. P. Machine Learning Configuration Interaction. *J. Chem. Theory Comput.* **2018**, *14*, 5739–5749.
- (50) Holmes, A. A.; Tubman, N. M.; Umrigar, C. J. Heat-bath configuration interaction: an efficient selected configuration interaction algorithm inspired by heat-bath sampling. *J. Chem. Theory Comput.* **2016**, *12*, 3674–3680.
- (51) Garniron, Y.; Scemama, A.; Loos, P.-F.; Caffarel, M. Hybrid stochastic-deterministic calculation of the second-order perturbative contribution of multireference perturbation theory. *J. Chem. Phys.* **2017**, *147*, 034101.
- (52) Holmes, A. A.; Umrigar, C. J.; Sharma, S. Excited states using semistochastic heat-bath configuration interaction. *J. Chem. Phys.* **2017**, *147*, 164111.
- (53) Sharma, S.; Holmes, A. A.; Jeanmairet, G.; Alavi, A.; Umrigar, C. J. Semistochastic Heat-Bath Configuration Interaction Method: Selected Configuration Interaction with Semistochastic Perturbation Theory. *J. Chem. Theory Comput.* **2017**, *13*, 1595–1604.
- (54) Chien, A. D.; Holmes, A. A.; Otten, M.; Umrigar, C. J.; Sharma, S.; Zimmerman, P. M. Excited States of Methylene, Polyenes, and Ozone from Heat-Bath Configuration Interaction. *J. Phys. Chem. A* **2018**, *122*, 2714–2722.

- (55) Yao, Y.; Giner, E.; Li, J.; Toulouse, J.; Umrigar, C. Almost exact energies for the Gaussian-2 set with the semistochastic heat-bath configuration interaction method. *J. Chem. Phys.* **2020**, *153*, 124117.
- (56) Evangelista, F. A. Adaptive multiconfigurational wave functions. *J. Chem. Phys.* **2014**, *140*, 124114.
- (57) Schriber, J. B.; Evangelista, F. A. Communication: An adaptive configuration interaction approach for strongly correlated electrons with tunable accuracy. *J. Chem. Phys.* **2016**, *144*, 161106.
- (58) Schriber, J. B.; Evangelista, F. A. Adaptive configuration interaction for computing challenging electronic excited states with tunable accuracy. *J. Chem. Theory Comput.* **2017**, *13*, 5354–5366.
- (59) Schriber, J. B.; Hannon, K. P.; Li, C.; Evangelista, F. A. A Combined Selected Configuration Interaction and Many-Body Treatment of Static and Dynamical Correlation in Oligoacenes. *J. Chem. Theory Comput.* **2018**, *14*, 6295–6305.
- (60) Tubman, N. M.; Lee, J.; Takeshita, T. Y.; Head-Gordon, M.; Whaley, K. B. A deterministic alternative to the full configuration interaction quantum Monte Carlo method. *J. Chem. Phys.* **2016**, *145*, 044112.
- (61) Lehtola, S.; Tubman, N. M.; Whaley, K. B.; Head-Gordon, M. Cluster decomposition of full configuration interaction wave functions: A tool for chemical interpretation of systems with strong correlation. *J. Chem. Phys.* **2017**, *147*, 154105.
- (62) Tubman, N. M.; Freeman, C. D.; Levine, D. S.; Hait, D.; Head-Gordon, M.; Whaley, K. B. Modern approaches to exact diagonalization and selected configuration interaction with the adaptive sampling CI method. *J. Chem. Theory Comput.* **2020**, *16*, 2139–2159.

- (63) Tubman, N. M.; Levine, D. S.; Hait, D.; Head-Gordon, M.; Whaley, K. B. An efficient deterministic perturbation theory for selected configuration interaction methods. **2018**, arXiv preprint arXiv:1808.02049.
- (64) Liu, W.; Hoffmann, M. R. SDS: the ‘static-dynamic-static’ framework for strongly correlated electrons. *Theor. Chem. Acc.* **2014**, *133*, 1481.
- (65) Lei, Y.; Liu, W.; Hoffmann, M. R. Further development of SDSPT2 for strongly correlated electrons. *Mol. Phys.* **2017**, *115*, 2696–2707.
- (66) Zhang, N.; Liu, W.; Hoffmann, M. R. Iterative Configuration Interaction with Selection. *J. Chem. Theory Comput.* **2020**, *16*, 2296–2316.
- (67) Garniron, Y.; Scemama, A.; Giner, E.; Caffarel, M.; Loos, P.-F. Selected configuration interaction dressed by perturbation. *J. Chem. Phys.* **2018**, *149*, 064103.
- (68) Wang, Z.; Li, Y.; Lu, J. Coordinate descent full configuration interaction. *J. Chem. Theory Comput.* **2019**, *15*, 3558–3569.
- (69) Giner, E.; Assaraf, R.; Toulouse, J. Quantum Monte Carlo with reoptimised perturbatively selected configuration-interaction wave functions. *Mol. Phys.* **2016**, *114*, 910–920.
- (70) Scemama, A.; Benali, A.; Jacquemin, D.; Caffarel, M.; Loos, P.-F. Excitation energies from diffusion Monte Carlo using selected configuration interaction nodes. *J. Chem. Phys.* **2018**, *149*, 034108.
- (71) Bender, C. F.; Davidson, E. R. Studies in configuration interaction: The first-row diatomic hydrides. *Phys. Rev.* **1969**, *183*, 23.
- (72) Whitten, J. L.; Hackmeyer, M. Configuration interaction studies of ground and excited states of polyatomic molecules. I. The CI formulation and studies of formaldehyde. *J. Chem. Phys.* **1969**, *51*, 5584–5596.

- (73) Huron, B.; Malrieu, J. P.; Rancurel, P. Iterative perturbation calculations of ground and excited state energies from multiconfigurational zeroth-order wave functions. *J. Chem. Phys.* **1973**, *58*, 5745–5759.
- (74) Evangelisti, S.; Daudey, J. P.; Malrieu, J. P. Convergence of an improved CIPSI algorithm. *Chem. Phys.* **1983**, *75*, 91–102.
- (75) Buenker, R. J.; Peyerimhoff, S. D. Individualized configuration selection in CI calculations with subsequent energy extrapolation. *Theor. Chem. Acta* **1974**, *35*, 33–58.
- (76) Eriksen, J. J.; Anderson, T. A.; Deustua, J. E.; Ghanem, K.; Hait, D.; Hoffmann, M. R.; Lee, S.; Levine, D. S.; Magoulas, I.; Shen, J.; Tubman, N. M.; Whaley, K. B.; Xu, E.; Yao, Y.; Zhang, N.; Alavi, A.; Chan, G. K.-L.; Head-Gordon, M.; Liu, W.; Piecuch, P.; Sharma, S.; Ten-no, S. L.; Umrigar, C. J.; Gauss, J. The ground state electronic energy of benzene. *J. Phys. Chem. Lett.* **2020**, *11*, 8922–8929.
- (77) Detail of timsort. <https://en.wikipedia.org/wiki/Timsort>.
- (78) <https://github.com/timsort/cpp-TimSort>.
- (79) Buenker, R. J. In *Molecular Physics and Quantum Chemistry: into the 80's*; Burton, P. G., Ed.; University of Wollongong Press: Wollongong, Australia, 1980; pp 1.5.1–1.5.37.
- (80) Buenker, R. J. Combining perturbation theory techniques with variational CI calculations to study molecular excited states. *Int. J. Quantum Chem.* **1986**, *29*, 435–460.
- (81) Krebs, S.; Buenker, R. J. A new table-direct configuration interaction method for the evaluation of Hamiltonian matrix elements in a basis of linear combinations of spin-adapted functions. *J. Chem. Phys.* **1995**, *103*, 5613–5629.
- (82) Khait, Y. G.; Hoffmann, M. R. *Low-Lying Potential Energy Surfaces*; Chapter 8, pp 176–198.

- (83) Huang, C.; Liu, W.; Xiao, Y.; Hoffmann, M. R. iVI: An iterative vector interaction method for large eigenvalue problems. *J. Comput. Chem.* **2017**, *38*, 2481–2499, (E) **2018**, *39*, 338.
- (84) Song, Y.; Guo, Y.; Lei, Y.; Liu, W. Benchmarking SDSPT2 and SDSCI for low-lying excited states of closed- and open-shell organic molecules. (unpublished).
- (85) Huang, C.; Liu, W. iVI-TD-DFT: An iterative vector interaction method for exterior/interior roots of TD-DFT. *J. Comput. Chem.* **2019**, *40*, 1023–1037, (E) **2018**, *39*, 338.
- (86) Paldus, J. Group theoretical approach to the configuration interaction and perturbation theory calculations for atomic and molecular systems. *J. Chem. Phys.* **1974**, *61*, 5321–5330.
- (87) Paldus, J.; Boyle, M. J. Unitary group approach to the many-electron correlation problem via graphical methods of spin algebras. *Phys. Script.* **1980**, *21*, 295–311.
- (88) Shavitt, I. In *The Unitary Group for the Evaluation of Electronic Energy Matrix Elements*, 1st ed.; Hinze, J., Ed.; Lecture Notes in Chemistry 22; Springer-Verlag Berlin Heidelberg, 1981; pp 1–50.
- (89) Shavitt, I. Graph theoretical concepts for the unitary group approach to the many-electron correlation problem. *Int. J. Quantum Chem., Symp.* **1977**, *12*, 131–148.
- (90) Duch, W.; Karwowski, J. Symmetric group approach to configuration interaction methods. *Comp. Phys. Rep.* **1985**, *2*, 93–170.
- (91) Shavitt, I. Matrix element evaluation in the unitary group approach to the electron correlation problem. *Int. J. Quantum Chem.* **1978**, *14*, 5–32.
- (92) Stampfuß, P.; Wenzel, W. Improved implementation and application of the individually selecting configuration interaction method. *J. Chem. Phys.* **2005**, *122*, 024110.

- (93) Smith, J. E. T.; Mussard, B.; Holmes, A. A.; Sharma, S. Cheap and near exact CASSCF with large active spaces. *J. Chem. Theory Comput.* **2017**, *13*, 5468–5478.
- (94) Li, J.; Yao, Y.; Holmes, A. A.; Otten, M.; Sun, Q.; Sharma, S.; Umrigar, C. J. Accurate many-body electronic structure near the basis set limit: Application to the chromium dimer. *Phys. Rev. Research* **2020**, *2*, 012015(R).
- (95) Schäfer, A.; Horn, H.; Ahlrichs, R. Fully optimized contracted Gaussian basis sets for atoms Li to Kr. *J. Chem. Phys.* **1992**, *97*, 2571–2577.
- (96) Liu, W.; Hong, G.; Dai, D.; Li, L.; Dolg, M. The Beijing 4-component density functional theory program package (BDF) and its application to EuO, EuS, YbO and YbS. *Theor. Chem. Acc.* **1997**, *96*, 75–83.
- (97) Liu, W.; Wang, F.; Li, L. *J. Theor. Comput. Chem.* **2003**, *2*, 257–272.
- (98) Liu, W.; Wang, F.; Li, L. In *Recent Advances in Relativistic Molecular Theory*; Hirao, K., Ishikawa, Y., Eds.; World Scientific: Singapore, 2004; pp 257–282.
- (99) Liu, W.; Wang, F.; Li, L. In *Encyclopedia of Computational Chemistry*; von Ragué Schleyer, P., Allinger, N. L., Clark, T., Gasteiger, J., Kollman, P. A., Schaefer III, H. F., Eds.; Wiley: Chichester, UK, 2004.
- (100) Zhang, Y.; Suo, B.; Wang, Z.; Zhang, N.; Li, Z.; Lei, Y.; Zou, W.; Gao, J.; Peng, D.; Pu, Z.; Xiao, Y.; Sun, Q.; Wang, F.; Ma, Y.; Wang, X.; Guo, Y.; Liu, W. BDF: A relativistic electronic structure program package. *J. Chem. Phys.* **2020**, *152*, 064113.
- (101) Booth, G. H.; Smart, S. D.; Alavi, A. Linear-scaling and parallelisable algorithms for stochastic quantum chemistry. *Mol. Phys.* **2014**, *112*, 1855–1869.
- (102) Li, J.; Otten, M.; Holmes, A. A.; Sharma, S.; Umrigar, C. J. Fast semistochastic heat-bath configuration interaction. *J. Chem. Phys.* **2018**, *149*, 214110.

- (103) Guo, S.; Li, Z.; Chan, G. K.-L. A Perturbative Density Matrix Renormalization Group Algorithm for Large Active Spaces. *J. Chem. Theory Comput.* **2018**, *14*, 4063–4071.
- (104) Li, Z.; Xiao, Y.; Liu, W. On the spin separation of algebraic two-component relativistic Hamiltonians. *J. Chem. Phys.* **2012**, *137*, 154114.
- (105) Li, Z.; Xiao, Y.; Liu, W. On the spin separation of algebraic two-component relativistic Hamiltonians: Molecular properties. *J. Chem. Phys.* **2014**, *141*, 054111.
- (106) Balabanov, N. B.; Peterson, K. A. Systematically convergent basis sets for transition metals. I. All-electron correlation consistent basis sets for the 3d elements Sc–Zn. *J. Chem. Phys.* **2005**, *123*, 064107.
- (107) Li, Z. (*private communication*).